and its high prevalence among MSM, this strain may have acquired higher infectivity and efficient transmission through sexual contact.

Another issue we wanted to clarify in this study was the transmission of antiviral drug resistance. We found no antiretroviral resistance in the 26 sequenced cases. On the other hand, we detected two cases with a mutation combination of rtV173L + rtL180M + rtM204V in HBV reverse transcriptase, demonstrating resistance against lamivudine-emtricitabine. One patient was antiretroviral therapy naïve; thus, transmission of drug-resistant HBV is strongly suspected. It is peculiar that the isolate harboring the drug-resistant mutations in HBV was a singleton, considering that genetically identical isolates were prevailing, that there were very low mutation rates that suggest few chances of reverting to wild type, and that there were actively ongoing *de novo* infections. This finding might be due to resistant viruses being masked by wild-type viruses under untreated conditions, as reported in the case of HIV-1 drug resistance (6). The possibility of minority resistance populations of HBV could be verified by detection with a highly sensitive method.

In conclusion, we clarified the molecular epidemiology of HBV/HIV-1 coinfection in Japan. Our data suggest that ongoing HBV infections lie outside prevention programs targeting the MTCT and blood transfusion infection routes, and they suggest the urgent need for new prevention strategies focusing on the high-risk group of the HIV-1-seropositive MSM population.

ACKNOWLEDGMENTS

This study was supported by a Research Grant for Research on HIV/AIDS from the Ministry of Health, Labor, and Welfare of Japan (no. H19-AIDS-007, H21-AIDS-005, and H22-AIDS-004).

We thank Yasuhito Tanaka, Nagoya City University Graduate School of Medical Sciences, for helpful discussion and Claire Baldwin for help in preparing the manuscript.

REFERENCES

1. **Allen, M. I., et al.** 1998. Identification and characterization of mutations in hepatitis B virus resistant to lamivudine. Lamivudine Clinical Investigation Group. Hepatology **27:**1670–1677.
2. **Angus, P., et al.** 2003. Resistance to adefovir dipivoxil therapy associated with the selection of a novel mutation in the HBV polymerase. Gastroenterology **125:**292–297.
3. **Drummond, A. J., S. Y. Ho, M. J. Phillips, and A. Rambaut.** 2006. Relaxed phylogenetics and dating with confidence. PLoS Biol. **4:**e88.
4. **Drummond, A. J., and A. Rambaut.** 2007. BEAST: Bayesian evolutionary analysis by sampling trees. BMC Evol. Biol. **7:**214.
5. **Gatanaga, H., et al.** 2007. Drug-resistant HIV-1 prevalence in patients newly diagnosed with HIV/AIDS in Japan. Antiviral Res. **75:**75–82.
6. **Harrigan, P. R., S. Bloor, and B. A. Larder.** 1998. Relative replicative fitness of zidovudine-resistant human immunodeficiency virus type 1 isolates in vitro. J. Virol. **72:**3773–3778.
7. **Johnson, V. A., et al.** 2009. Update of the drug resistance mutations in HIV-1: December 2009. Top. HIV Med. **17:**138–145.
8. **Koibuchi, T., et al.** 2001. Predominance of genotype A HBV in an HBV-HIV-1 dually positive population compared with an HIV-1-negative counterpart in Japan. J. Med. Virol. **64:**435–440.
9. **Matsuura, K., et al.** 2009. Distribution of hepatitis B virus genotypes among patients with chronic infection in Japan shifting toward an increase of genotype A. J. Clin. Microbiol. **47:**1476–1483.
10. **Michitaka, K., et al.** 2006. Tracing the history of hepatitis B virus genotype D in western Japan. J. Med. Virol. **78:**44–52.
11. **Miyakawa, Y., and M. Mizokami.** 2003. Classifying hepatitis B virus genotypes. Intervirology **46:**329–338.
12. **Norder, H., et al.** 2004. Genetic diversity of hepatitis B virus strains derived worldwide: genotypes, subgenotypes, and HBsAg subtypes. Intervirology **47:**289–309.
13. **Noto, H., et al.** 2003. Combined passive and active immunoprophylaxis for preventing perinatal transmission of the hepatitis B virus carrier state in Shizuoka, Japan during 1980–1994. J. Gastroenterol. Hepatol. **18:**943–949.
14. **Nylander, J.** 2004. MrModeltest v2. Uppsala University, Uppsala, Sweden.
15. **Oda, T.** 2000. Further decline of hepatitis B surface antigen (HBsAg) prevalence in Japan. Jpn. J. Cancer Res. **91:**361.
16. **Okada, K., I. Kamiyama, M. Inomata, M. Imai, and Y. Miyakawa.** 1976. e antigen and anti-e in the serum of asymptomatic carrier mothers as indicators of positive and negative transmission of hepatitis B virus to their infants. N. Engl. J. Med. **294:**746–749.
17. **Orito, E., et al.** 2001. Geographic distribution of hepatitis B virus (HBV) genotype in patients with chronic HBV infection in Japan. Hepatology **34:** 590–594.
18. **Osiowy, C., E. Giles, Y. Tanaka, M. Mizokami, and G. Y. Minuk.** 2006. Molecular evolution of hepatitis B virus over 25 years. J. Virol. **80:**10307–10314.
19. **Pybus, O. G., A. J. Drummond, T. Nakano, B. H. Robertson, and A. Rambaut.** 2003. The epidemiology and iatrogenic transmission of hepatitis C virus in Egypt: a Bayesian coalescent approach. Mol. Biol. Evol. **20:**381–387.
20. **Quarleri, J., et al.** 2007. Hepatitis B virus genotype distribution and its lamivudine-resistant mutants in HIV-coinfected patients with chronic and occult hepatitis B. AIDS Res. Hum. Retroviruses **23:**525–531.
21. **Rambout, A., and A. J. Drummond.** 2007. Tracer v1.4. Institute of Evolutionary Biology, University of Edinburgh, Edinburgh, Scotland. http://tree.bio.ed.ac.uk.
22. **Schaefer, S.** 2007. Hepatitis B virus taxonomy and hepatitis B virus genotypes. World J. Gastroenterol. **13:**14–21.
23. **Shafer, R.** 2010, posting date. Stanford drug resistance database. http://hivdb.stanford.edu/.
24. **Sheldon, J., et al.** 2005. Selection of hepatitis B virus polymerase mutations in HIV-coinfected patients treated with tenofovir. Antivir. Ther. **10:**727–734.
25. **Shiraki, K.** 2000. Perinatal transmission of hepatitis B virus and its prevention. J. Gastroenterol. Hepatol. **15**(Suppl.)**:**E11–E15.
26. **Soriano, V., et al.** 2010. Predictors of hepatitis B virus genotype and viraemia in HIV-infected patients with chronic hepatitis B in Europe. J. Antimicrob. Chemother. **65:**548–555.
27. **Sugauchi, F., et al.** 2001. A novel variant genotype C of hepatitis B virus identified in isolates from Australian Aborigines: complete genome sequence and phylogenetic relatedness. J. Gen. Virol. **82:**883–892.
28. **Suzuki, Y., et al.** 2005. Persistence of acute infection with hepatitis B virus genotype A and treatment in Japan. J. Med. Virol. **76:**33–39.
29. **Swafford, D.** 2003. PAUP. Phylogenetic analysis using parsimony (and other methods), version 4. Sinouer Associates, Sunderland, MA.
30. **Takeda, Y., et al.** 2006. Difference of HBV genotype distribution between acute hepatitis and chronic hepatitis in Japan. Infection **34:**201–207.
31. **Tanaka, J., et al.** 2004. Sex- and age-specific carriers of hepatitis B and C viruses in Japan estimated by the prevalence in the 3,485,648 first-time blood donors during 1995-2000. Intervirology **47:**32–40.
32. **Tenney, D. J., et al.** 2004. Clinical emergence of entecavir-resistant hepatitis B virus requires additional substitutions in virus already resistant to lamivudine. Antimicrob. Agents Chemother. **48:**3498–3507.
33. **Trimoulet, P., et al.** 2007. Hepatitis B virus genotypes: a retrospective survey in southwestern France, 1999-2004. Gastroenterol. Clin. Biol. **31:**1088–1094.
34. **Westland, C. E., et al.** 2003. Week 48 resistance surveillance in two phase 3 clinical studies of adefovir dipivoxil for chronic hepatitis B. Hepatology **38:**96–103.
35. **Yang, H., et al.** 2002. Resistance surveillance in chronic hepatitis B patients treated with adefovir dipivoxil for up to 60 weeks. Hepatology **36:**464–473.
36. **Yotsuyanagi, H., et al.** 2005. Distinct geographic distributions of hepatitis B virus genotypes in patients with acute infection in Japan. J. Med. Virol. **77:**39–46.

Bioorganic & Medicinal Chemistry 19 (2011) 6735–6742

Contents lists available at SciVerse ScienceDirect

Bioorganic & Medicinal Chemistry

journal homepage: www.elsevier.com/locate/bmc

Small molecular CD4 mimics as HIV entry inhibitors

Tetsuo Narumi [a], Hiroshi Arai [a], Kazuhisa Yoshimura [b], Shigeyoshi Harada [b], Wataru Nomura [a], Shuzo Matsushita [b], Hirokazu Tamamura [a,*]

[a] Institute of Biomaterials and Bioengineering, Tokyo Medical and Dental University, Chiyoda-ku, Tokyo 101-0062, Japan
[b] Center for AIDS Research, Kumamoto University, Kumamoto 860-0811, Japan

ARTICLE INFO

Article history:
Received 5 August 2011
Revised 23 September 2011
Accepted 24 September 2011
Available online 29 September 2011

Keywords:
CD4 mimic
HIV entry
gp120-CD4 interaction
Phe43 cavity

ABSTRACT

Derivatives of CD4 mimics were designed and synthesized to interact with the conserved residues of the Phe43 cavity in gp120 to investigate their anti-HIV activity, cytotoxicity, and CD4 mimicry effects on conformational changes of gp120. Significant potency gains were made by installation of bulky hydrophobic groups into the piperidine moiety, resulting in discovery of a potent compound with a higher selective index and CD4 mimicry. The current study identified a novel lead compound **11** with significant anti-HIV activity and lower cytotoxicity than those of known CD4 mimics.

1. Introduction

The dynamic supramolecular mechanism of HIV cellular invasion has emerged as a key target for blocking HIV entry into host cells.[1] HIV entry begins with the interaction of a viral envelope glycoprotein gp120 and a cell surface protein CD4.[2] This triggers extensive conformational changes in gp120 exposing co-receptor binding domains and allowing the subsequent binding of gp120 to a co-receptor, CCR5[3]/CXCR4.[4] Following the viral attachment and co-receptor binding, gp41, another viral envelope glycoprotein mediates the fusion of the viral and cell membranes, thus completing the infection. Molecules interacting with each of these steps are potential candidates for anti-HIV-1 drugs. In particular, discovery and development of novel drugs that inhibit the viral attachment are required for blocking the HIV infection at an early stage.[5]

In 2005, small molecular CD4 mimics targeting the viral attachment were identified by an HIV syncytium formation assay and shown to bind within the Phe43 cavity, a highly conserved pocket on gp120,[6] which is a hydrophobic cavity occupied by the aromatic ring of Phe43 of CD4.[7] These molecules are comprised of three essential moieties: an aromatic ring, an oxalamide linker, and a piperidine ring (Fig. 1) and show micromolar order potency against diverse HIV-1 strains including laboratory and primary isolates. Furthermore, they possess the unique ability to induce the conformational changes in gp120 required for binding with soluble CD4.[8] Such CD4 mimicry can be an advantage for rendering the envelope more sensitive to neutralizing antibodies.[9] While such properties are promising for the development of HIV entry inhibitors and the use combinatorially with neutralizing antibodies, cytotoxicity is one of the drawbacks of CD4 mimics.

To date, we and others have performed structure–activity relationship (SAR) studies of CD4 mimics based on modifications of the aromatic ring, the oxalamide linker, and the piperidine moiety of CD4 mimics. In an initial survey of SAR studies of NBD-556 and NBD-557, Madani et al. revealed that potency (i.e., CD4 binding and mimicry) was highly sensitive to modifications of the aromatic ring, which is thought to bind in the Phe43 cavity of gp120 (Fig. 1). The CD4 mimic analogs (JRC-II-191) with a *para*-chloro-*meta*-fluorophenyl ring had significantly increased affinity for gp120.[10] Our SAR studies also revealed that a certain size and electron-withdrawing ability of the *para*-substituents are indispensable for potent anti-HIV activity.[11] Furthermore, the replacement of the chlorine group at the *para* position with a methyl group which is almost as bulky as a bromine atom leads to improvement of solubility of the compounds in buffer to provide the reproducibility in the biological studies with comparable biological activities.

Further SAR studies were focused on the piperidine moiety of CD4 mimics to investigate its contribution to biological activities, and we found that the piperidine ring is critical for the CD4 mimicry on the conformational changes in gp120 and that substituents on the nitrogen of the piperidine moiety can contribute significantly to both anti-HIV activity and cytotoxicity.[12] Based on these SARs and our modeling study, we speculate that interactions of the piperidine moiety with several amino acids in the vicinity of the Phe43 cavity in gp120, specifically an electrostatic interaction with

* Corresponding author. Tel.: +81 3 5280 8036; fax: +81 3 5280 8039.
E-mail address: tamamura.mr@tmd.ac.jp (H. Tamamura).

0968-0896/$ - see front matter © 2011 Elsevier Ltd. All rights reserved.
doi:10.1016/j.bmc.2011.09.045

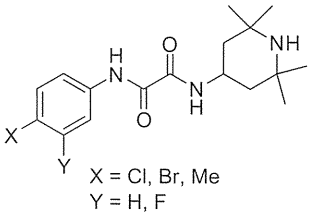

Figure 1. CD4 mimics.

Asp368 and a hydrophobic interaction with Val430, are critical for biological activity. LaLonde et al. focused on modifications of the piperidine moiety using computational approaches, adducing evidence for the importance of these interactions to the binding affinity against gp120.[13] Based on these results, we envisioned that an enhancement of the interaction of CD4 mimics with residues associated with the Phe43 cavity in gp120 would lead to the increase of their potency and CD4 mimicry inducing the conformational changes of gp120, and the decrease of their cytotoxicity. Thus, in this study a series of CD4 mimics, which were designed to interact with the conserved residues in the Phe43 cavity, were synthesized to increase binding affinity for gp120, and the appropriate SAR studies were performed.

2. Results and discussion

Two types of CD4 mimic analogs were designed: (1) CD4 mimics with the ability to interact electrostatically with Asp368, and (2) CD4 mimics with the ability to interact hydrophobically with Val430 (Fig. 2). The X-ray structure of gp120 bound to soluble CD4 (PDB: 1RZJ) revealed that the guanidino group of Arg59 of CD4 is involved in a hydrogen bond with Asp368 of gp120. In order to mimic this interaction, a guanidino and related groups such as thiourea and urea were introduced to the piperidine moiety of the CD4 mimic derivative COC-021, which was developed in order to modify the nitrogen of the piperidine moiety and which showed biological activity, including anti-HIV activity and CD4 mimicry, similar to that of the parent compound NBD-556.[12] Furthermore, to interact with Val430 by hydrophobic interaction, the methyl groups on the piperidine ring were replaced with cyclohexyl groups to prepare a novel CD4 mimic analog with enhanced hydrophobicity.

2.1. Chemistry

The syntheses of CD4 mimics are outlined in Scheme 1. CD4 mimics with guanidine, thiourea, and urea groups on the piperidine moiety were prepared using our previously reported method.[12] Coupling of *p*-chloroaniline with ethyl chloroglyoxylate followed by aminolysis of the ethyl ester with 4-amino-*N*-benzylpiperidine under microwave conditions (150 °C, 3 h) gave the corresponding amide. Removal of the benzyl group with 1-chloroethyl chloroformate[14] gave the free piperidine moiety, which was modified to produce the desired compounds **4–8** (Scheme 1).

For synthesis of a CD4 mimic derivative with two cyclohexyl groups, treatment of 2,2,6,6-tetramethylpiperidin-4-one **9** with cyclohexanone in the presence of ammonium chloride furnished a 2,6-substituted piperidin-4-one derivative,[15] and reductive amination with benzylamine and subsequent removal of benzyl group provided a primary amine **10**. Microwave-assisted aminolysis of ester **2** with amine **10** yielded the desired dicyclohexyl-substituted analog **11** (Scheme 2). The synthesis of the other compounds is described in Supplementary data.

2.2. Biological studies

The anti-HIV activity of synthetic CD4 mimics was evaluated in a single-round viral infective assay. Inhibition of HIV-1 infection was measured as reduction in β-galactosidase gene expression after a single-round of virus infection of TZM-bl cells as described previously.[9] IC_{50} was defined as the concentration that caused a 50% reduction in the β-galactosidase activity (relative light units [RLU]) compared to virus control wells. Cytotoxicity

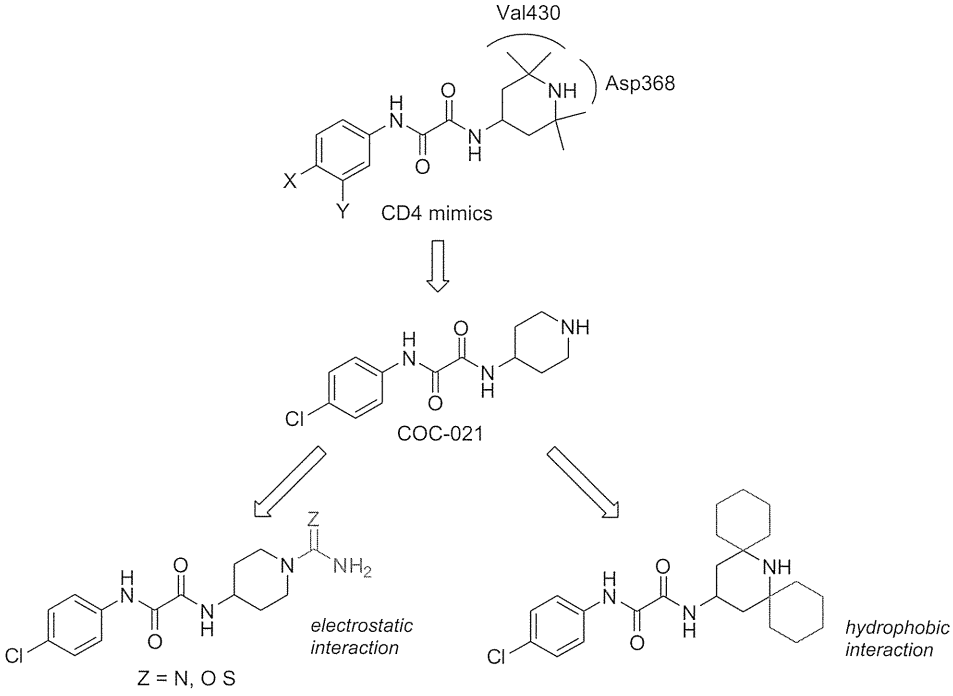

Figure 2. Design strategy for novel CD4 mimics with enhanced electrostatic/hydrophobic interaction.

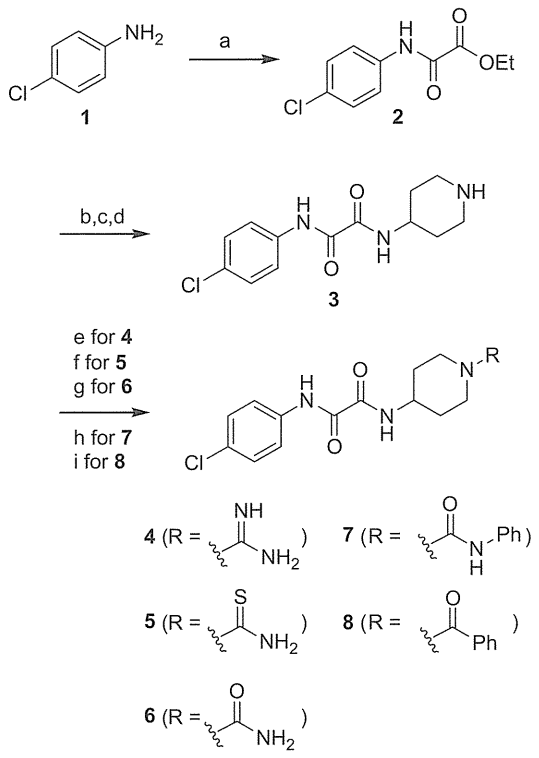

Scheme 1. Synthesis of N-modified piperidine derivatives **4–8**. Reagents and conditions: (a) Ethyl chloroglyoxylate, Et_3N, THF, quant.; (b) 1-benzyl-4-aminopiperidine, Et_3N, EtOH, 150 °C, microwave, 78%; (c) 1-chloroethyl chloroformate, CH_2Cl_2; (d) MeOH, reflux, 64% in two steps; (e) 1*H*-pyrazole-1-carboxamidine hydrochloride, Et_3N, DMF, 61%; (f) (trimethylsilyl)isothiocyanate, $CHCl_3$, 36%; (g) (trimethylsilyl)isocyanate, $CHCl_3$, 30%; (h) phenyl isocyanate, $CHCl_3$, 32%, (i) benzoyl chloride, Et_3N, CH_2Cl_2, 68%.

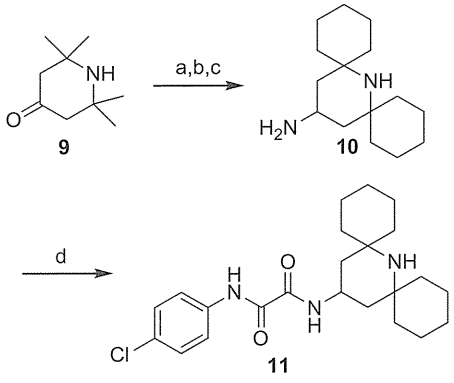

Scheme 2. Synthesis of dicyclohexyl derivative **11**. Reagents and conditions: (a) Cyclohexanone, NH_4Cl, DMSO, 60 °C; (b) benzylamine, $NaBH_4$, MeOH; (c) 10% Pd/C, H_2, MeOH, 7% from **9**; (d) **2**, Et_3N, EtOH, 150 °C, microwave, 17%.

of the compounds based on the viability of mock-infected PM1/CCR5 cells was evaluated using WST-8 method. The assay results for the CD4 mimics **3–8** are shown in Table 1. Compound **12** (NBD-556) showed potent anti-HIV activity; its IC_{50} value was 0.61 μM, and it is thus 13–20-fold more potent than the reported values.[11,12] Although previous studies found that compound **13**, with a methyl group at the *p*-position of the phenyl ring, and compound **3**, with no dimethyl groups on the piperidine ring, showed potent anti-HIV activity, only moderate activities were observed in the current study; this is about 12–14-fold less potency than reported for compound **12** and is probably due to

Table 1
Effects of the nitrogen-substituents on anti-HIV activity and cytotoxicity of CD4 mimic analogs[a]

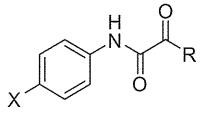

Compd	X	R	IC_{50}[b] (μM)	CC_{50}[c] (μM)	SI (CC_{50}/IC_{50})
		YTA (R5)			
3[d]	Cl	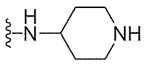	7.0	51	7.3
4[e]	Cl	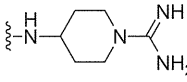	6.1	72	12
5	Cl	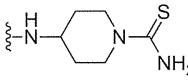	5.5	42	7.6
6	Cl	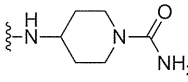	8.3	310	37
7	Cl	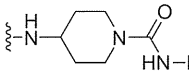	11	6.2	0.56
8	Cl	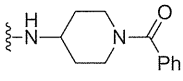	5.1	ND	–
12 (NBD-556)	Cl	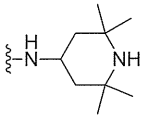	0.61	35	57
13	Me	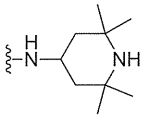	8.4	260	31

[a] All data with standard deviation are the mean values for at least three independent experiments (ND = not determined)
[b] IC_{50} values are based on the reduction in the β-galactosidase activity in TZM-bl cells.
[c] CC_{50} values are based on the reduction of the viability of mock-infected PM1/CCR5 cells.
[d] Desalted by satd $NaHCO_3$ aq.
[e] TFA salts.

the different assay system. All of the synthesized novel derivatives of compound **12** showed moderate to potent anti-HIV activity. A guanidine derivative **4** and thiourea derivative **5** showed potent anti-HIV activities (IC_{50} of **4** = 6.1 μM and IC_{50} of **5** = 5.5 μM) but their potency was approximately 10-fold lower than that of the parent compound **12**. A urea derivative **6** also showed potent anti-HIV activity (IC_{50} = 8.3 μM) and exhibited lower cytotoxicity (CC_{50} = 310 μM). On the other hand, introduction of a phenyl group in the urea derivative **6**, led to an *N*-phenylurea derivative **7**, with an increase of cytotoxicity (CC_{50} = 6.2 μM). To examine the influence of the N–H group on anti-HIV activity, an *N*-benzoyl derivative **8** was also tested. The IC_{50} value of **8** was 5.1 μM, which is equipotent with the thioamide derivative **5**. The *N*-benzoyl derivative **8** was essentially equipotent with **3** and this result suggests the presence of the hydrogen atom of the N–H group does not contribute to an increase in anti-HIV activity. The thiourea derivative **5** and the *N*-phenylurea derivative **7**, which have more acidic protons (pK_a of thiourea and *N*-phenylurea; 21.0 and 19.5,[16] respectively) than the urea derivative **6** (pK_a of urea; 26.9[16]), were found to exhibit relatively strong cytotoxicity. This observation indicates that

Table 2
Anti-HIV activity and cytotoxicity of CD4 mimic analogs **11**, **12**, and **14–17**[a]

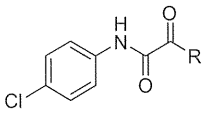

Compd	R	IC_{50}[b] (μM)	CC_{50}[c] (μM)	SI (CC_{50}/IC_{50})
		YTA (R5)		
11	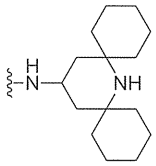	0.68	120	176
14	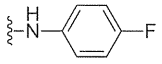	3.1	>500	>160
15	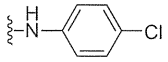	>100	>500	–
16	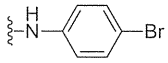	>100	>500	–
17	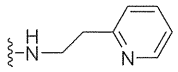	19.8	480	24
12 (NBD-556)	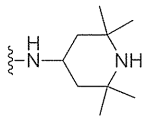	0.61	35	57

[a] All data with standard deviation are the mean values for at least three independent experiments
[b] IC_{50} values are based on the reduction in the β-galactosidase activity in TZM-bl cells.
[c] CC_{50} values are based on the reduction of the viability of mock-infected PM1/CCR5 cells.

Table 3
Anti-HIV activity of CD4 mimic **12** and dicyclohexyl derivative **11**[a]

Compd	R	IC_{50}[b] (μM) Single-round assay	IC_{50}[c] (μM) Multi-round assay
12 (NBD-556)	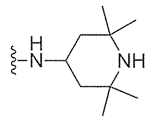	0.61	0.90
11	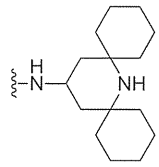	0.68	0.56

[a] All data with standard deviation are the mean values for at least three independent experiments.
[b] IC_{50} values of the single-round assay are based on the reduction in the β-galactosidase activity in TZM-bl cells.
[c] IC_{50} values of the multi-round assay are based on the inhibition of HIV-1-induced cytopathogenicity in PM1/CCR5 cells.

substitution on the piperidine moiety of acidic functional groups was unfavorable.

The assay results for CD4 mimics that target hydrophobic interactions are shown in Table 2. Compound **11** showed significant anti-HIV activity (IC_{50} = 0.68 μM) comparable to that of the lead compound **12**, but exhibited lower cytotoxicity. Compound **11** showed approximately four-fold less cytotoxicity than **12**. The SI of **11** is 176, 3 times higher than that of **12** (SI = 57). This result suggests that substitution of bulky hydrophobic groups into the piperidine moiety may be consistent with lower cytotoxicity of CD4 mimics. It is noteworthy that compound **14**, which has a *p*-fluoroanilino group in place of the piperidine ring, exhibits potent anti-HIV activity (IC_{50} = 3.1 μM) without significant cytotoxicity (CC_{50} >500 μM). The SI of compound **14** is >160, which is comparable to that of **11**. However, replacement of the piperidine moiety with a *p*-bromo- or *p*-chloroanilino group resulted in the loss of anti-HIV activity. These results suggest that the introduction of a fluorine atom to the piperidine moiety might be consistent with improvement of the anti-HIV activity. Extension of the alkyl chain by two carbons, as in **17** resulted in a 30-fold loss of anti-HIV activity, indicating that relatively rigid structures are preferable for anti-HIV activity.

The anti-HIV activities of **12** and compound **11**, which has a higher SI than the parent compound **12** were evaluated in a multi-round viral infective assay and the results are shown in Table 3. In this assay, the IC_{50} value of **12** was 0.90 μM, which was slightly larger value than measured in a single-round assay (IC_{50} = 0.61 μM). Compound **11** showed higher anti-HIV activity (IC_{50} = 0.56 μM) than compound **12**, indicating that the introduction of hydrophobic cyclohexyl groups into the piperdine moiety has a positive effect on not only the cytotoxicity but also the anti-HIV activity. This is possibly due to the stability in the assay condition derived from the hydrophobicity of cyclohexyl group(s). These results are consistent with a previous study of the analog with one hydrophobic *gem*-dimethyl group on the piperidine moiety, a compound with potent anti-HIV activity and efficient binding affinity for gp120.[13]

To gain insight into the interactions involved in the binding, molecular modeling of compound **11** docked into gp120 (1RZJ) was carried with Sybyl 7.1 (Fig. 3). The binding mode of compound **11** in the Phe43 cavity suggested that the orientation of the piperidine moiety of **11** is different from that in compound **12**, and that the cyclohexyl group can be positioned near Val430 with whose isopropyl group it can interact hydrophobically.

Fluorescence activated cell sorting (FACS) analysis was performed as previously reported,[11,12] to evaluate the CD4 mimicry effects on conformational changes of gp120 and the results are shown in Figure 4. Comparison of the binding of an anti-envelope CD4-induced monoclonal antibody (4C11) to the cell surface pretreated with the above CD4 mimics was measured in terms of the mean fluorescence intensity (MFI). Our previous studies revealed that the profile of the binding of 4C11 to the Env-expressing cell surface pretreated with compound **12** was entirely similar to that of pretreatment of soluble CD4. In this FACS analysis, the MFI of pretreatment with compound **12** is 23.13. The profiles of the binding of 4C11 to the cell surface pretreated with compounds **3**, **4** and **5** were comparable to that of compound **12** [MFI (**3**) = 20.54, MFI (**4**) = 20.85, MFI (**5**) = 20.24, respectively], suggesting that these derivatives offer a significant enhancement of binding affinity for 4C11. On the other hand, pretreatment with **6** and **8** did not cause significant enhancement of the binding affinity for 4C11, indicating that introduction of a carbonyl group on the piperidine nitrogen is not conducive to CD4 mimicry. The profile of the binding of 4C11 to the Env-expressing cell surface pretreated with compound **11**, which had significant anti-HIV activity and lower cytotoxicity than compound **12**, (MFI (**11**) = 22.17) was similar to that of compound **12**, suggesting that compound **11** offers significant enhancement of binding affinity for 4C11. This result indicates that compound **11** retains the CD4 mimicry on the conformational changes of gp120. Although compound **14** and compound **17** showed potent anti-HIV activity and no significant cytotoxicity, the profiles pretreated with (MFI (**14** and **17**) = 15.20 and 15.38) were similar to that of the control (MFI = 14.94), suggesting that these compounds **14** and **17** failed to produce a significant increase in binding affinity for 4C11. These

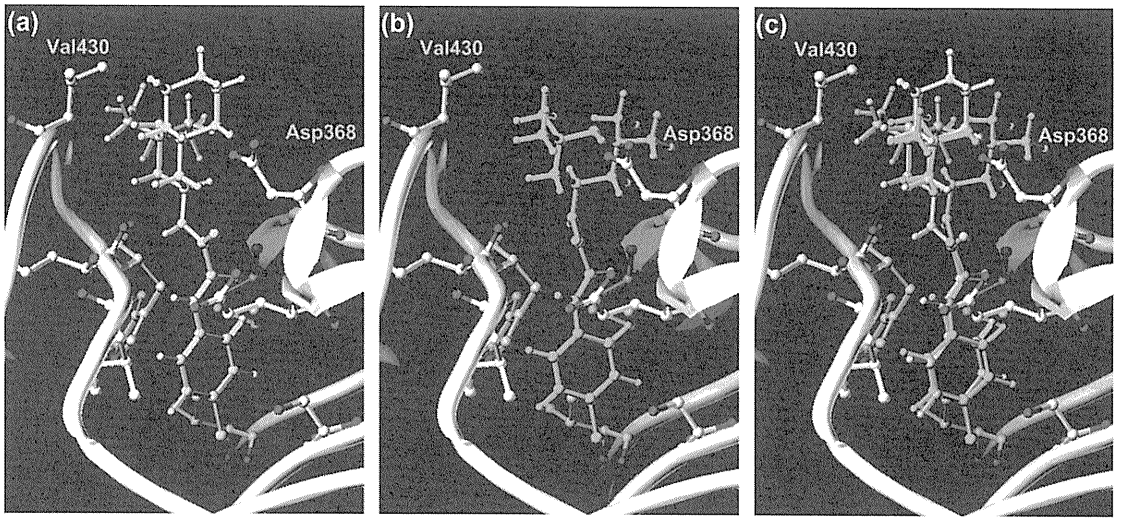

Figure 3. Docking structures of (a) compound **11** and (b) compound **12** bound in the Phe43 cavity of gp120 (1RZJ); (c) merge image of compounds **11** and **12**. Compounds **11** and **12** are represented in yellow and green sticks, respectively. Key residues in the cavity forming interactions with compounds are represented in gray sticks.

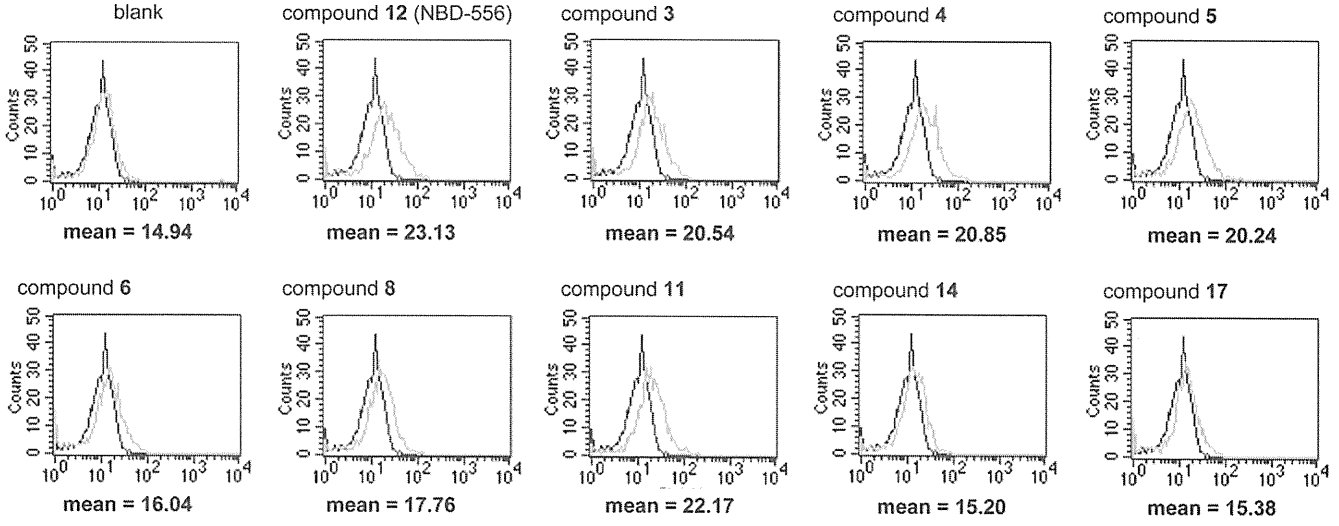

Figure 4. FACS analysis of compounds **12**, **3**–**6**, **8** (Table 1), **11**, **14**, and **17** (Table 2).

results are consistent with our previous finding that the piperidine ring is critical to the CD4 mimicry of the conformational changes in gp120.

3. Conclusion

A series of CD4 mimics were designed and synthesized to interact with the conserved residues in the Phe43 cavity of gp120 to investigate their anti-HIV activity, cytotoxicity, and CD4 mimicry as a function of conformational change of gp120. The biological activities of the synthetic compounds indicate that (1) the hydrogen atom of the piperidine moieties contributes significantly to cytotoxicity, and (2) installation of bulky hydrophobic groups into the piperidine moiety can increase anti-HIV activity and decrease cytotoxicity thus providing a novel compound with higher selective index than those of the original CD4 mimics. Furthermore, this modification has no great influence on the CD4 mimicry on the conformational change of gp120. Thus, compound **11** is promising for further studies. More detailed SAR investigations with respect to the substitution on the piperidine moiety have been ongoing studies.

4. Experimentals

^{1}H NMR and ^{13}C NMR spectra were recorded using a Bruker Avance III spectrometer. Chemical shifts are reported in δ (ppm) relative to Me_4Si (in $CDCl_3$) as internal standard. Low- and high-resolution mass spectra were recorded on a Bruker Daltonics microTOF focus in the positive and negative detection mode. For flash chromatography, Wakogel C-200 (Wako Pure Chemical Industries, Ltd) and silica gel 60 N (Kanto Chemical Co., Inc.) were employed. For analytical HPLC, a Cosmosil $5C_{18}$-ARII column (4.6 × 250 mm, Nacalai Tesque, Inc., Kyoto, Japan) was employed with a linear gradient of CH_3CN containing 0.1% (v/v) TFA at a flow rate of 1 cm^3 min^{-1} on a JASCO PU-2089 plus (JASCO Corporation, Ltd., Tokyo, Japan), and eluting products were detected by UV at 220 nm. Preparative HPLC was performed using a Cosmosil $5C_{18}$-ARII column (20 × 250 mm, Nacalai Tesque, Inc.) on a JASCO PU-2087 plus (JASCO Corporation, Ltd, Tokyo, Japan) in a suitable

gradient mode of CH_3CN solution containing 0.1% (v/v) TFA at a flow rate of 7 cm^3 min^{-1}. Microwave reactions were performed in Biotage Microwave Reaction Kit (sealed vials) in an Initiator™ (Biotage). The wattage was automatically adjusted to maintain the desired temperature for the desired period of time.

4.1. Chemistry

4.1.1. N^1-(4-Chlorophenyl)-N^2-(piperidin-4-yl)oxalamide (3)

To a stirred solution of *p*-choroaniline (**1**) (14.0 g, 110 mmol) in THF (146 mL) were added ethyl chloroglyoxylate (8.13 mL, 73.2 mmol) and triethylamine (Et_3N) (15.2 mL, 110 mmol) at 0 °C. The mixture was stirred for 6 h at room temperature. After the precipitate was filtrated off, the filtrate solution was concentrated under reduced pressure. The residue was dissolve in EtOAc, and washed with 1 M HCl, saturated $NaHCO_3$ and brine, then dried over $MgSO_4$. Concentration under reduced pressure gave the crude ethyl oxalamate, which was used without further purification. To a solution of the above ethyl oxalamate (1.27 g, 5.25 mmol) in EtOH (13.0 mL) were added Et_3N (1.46 mL, 10.5 mmol) and 4-amino-1-benzylpiperidine (2.97 mL, 15.8 mmol). The reaction mixture was stirred for 3 h at 150 °C under microwave irradiation. After being cooled to room temperature, the crystal was collected and washed with cold EtOH and *n*-hexane, and dried under reduced pressure to provide the corresponding amide (1.58 g, 81% yield) as colorless crystals. To a stirred solution of **S1** (1.46 g, 3.90 mmol) in CH_2Cl_2 (39.0 mL) was added dropwise 1-chloroethyl chloroformate (0.860 mL, 7.80 mmol) at 0 °C. After being stirred at room temperature for 30 min, the mixture was refluxed for 1 h. After concentration under reduced pressure, the residue was dissolved in MeOH and then refluxed for 1 h. After concentration under reduced pressure, the residue was diluted with EtOAc and washed with saturated $NaHCO_3$ and brine, then dried over $MgSO_4$. After concentration under reduced pressure, the residue was washed with cold EtOAc, and dried under reduced pressure to provide the title compound **3** (778 mg, 71% yield) as white powder.

^1H NMR (400 MHz, $CDCl_3$) δ 1.39–1.52 (m, 2H), 1.92–2.01 (m, 2H), 2.67–2.79 (m, 2H), 3.06–3.19 (m, 2H), 3.83–3.95 (m, 1H), 7.34 (d, J = 8.80 Hz, 2H), 7.44 (d, J = 7.64 Hz, 1H), 7.59 (d, J = 8.80 Hz, 2H), 9.28 (s, 1H); ^{13}C NMR (125 MHz, $CDCl_3$) δ 33.0 (2C), 45.2 (2C), 47.9, 21.0 (2C), 129.3 (2C), 130.5, 135.0, 157.6, 158.8; HRMS (ESI), *m/z* calcd for $C_{13}H_{17}ClN_3O_2$ (MH^+) 282.1004, found 282.1002.

4.1.2. N^1-(1-Carbamimidoylpiperidin-4-yl)-N^2-(4-chlorophenyl) oxalamide (4)

To a stirred solution of **3** (50.0 mg, 0.178 mmol) in DMF (20.0 mL) was added 1-aminopyrazole hydrochlride (312 mg, 2.13 mmol) and Et_3N (0.390 mL, 28.1 mmol). The reaction mixture was stirred at room temperature for 24 h. After concentration under reduced pressure, purification by preparative HPLC gave the trifluoroacetate of the title compound **4** as white powder (36.0 mg, 61% yield).

^1H NMR (500 MHz, DMSO) δ 1.41–1.55 (m, 2H), 1.59–1.71 (m, 2H), 2.70–2.74 (m, 2H), 3.74–3.87 (m, 1H), 3.88–4.03 (m, 2H), 5.93 (s, 2H), 7.42 (d, J = 9.00 Hz, 2H), 7.85 (d, J = 9.00 Hz, 2H), 8.95 (d, J = 9.00 Hz, 1H), 10.80 (s, 1H); ^{13}C NMR (125 MHz, DMSO) δ 31.3 (2C), 43.0 (2C), 47.6, 122.4 (2C), 128.6, 129.1 (2C), 137.1, 158.2, 159.3, 159.5; HRMS (ESI), *m/z* calcd for $C_{14}H_{19}ClN_5O_2$ (MH^+) 324.1222, found 324.1213.

4.1.3. N^1-(1-Carbamothioylpiperidin-4-yl)-N^2-(4-chlorophenyl) oxalamide (5)

To a stirred solution of **3** (140 mg, 0.498 mmol) in $CHCl_3$ (5.00 mL) was added trimethylsilyl isothiocyanate (141 mL, 1.00 mmol) and stirred at room temperature for 1 h. The precipitate was collected and washed with cold $CHCl_3$, and dried under reduced pressure to provide the title compound **5** as white powder. (62.0 mg, 36% yield).

^1H NMR (400 MHz, DMSO) δ 1.45–1.69 (m, 2H), 1.69–1.81 (m, 2H), 2.67–2.81 (m, 2H), 3.02–3.16 (m, 2H), 3.75–3.89 (m, 1H), 7.41 (d, J = 9.00 Hz, 2H), 7.85 (d, J = 9.00 Hz, 2H), 9.00 (d, J = 8.50 Hz, 1H), 10.80 (s, 1H); ^{13}C NMR (125 MHz, DMSO) δ 27.8 (2C), 42.3 (2C), 44.4, 122.0 (2C), 128.2, 128.6 (2C), 129.5, 136.6, 158.6, 159.4; Anal. calcd for $C_{14}H_{18}ClN_4O_2S$: C, 49.34; H, 5.03; N, 16.44. Found: C, 49.32; H, 4.76; N, 16.11.

4.1.4. N^1-(1-Carbamoylpiperidin-4-yl)-N^2-(4-chlorophenyl) oxalamide (6)

To a stirred solution of **3** (60.0 mg, 0.213 mmol) in $CHCl_3$ (1.10 mL) was added trimethylsilyl isocyanate (56.0 μL, 0.421 mmol), and the mixture was stirred at room temperature for 1 h. The precipitate was collected and washed with cold $CHCl_3$, and dried under reduced pressure to provide the title compound **6** (20.1 mg, 30% yield) as white powder.

^1H NMR (500 MHz, DMSO) δ 1.44–1.55 (m, 2H), 1.58–1.71 (m, 2H), 2.65–2.78 (m, 2H), 3.76–3.87 (m, 1H), 3.87–4.01 (m, 2H), 5.94 (s, 1H), 7.42 (d, J = 9.00 Hz, 2H), 7.86 (d, J = 9.00 Hz, 2H), 8.95 (d, J = 9.00 Hz, 1H), 10.80 (s, 1H); ^{13}C NMR (125 MHz, DMSO) δ 30.8 (2C), 42.6 (2C), 47.1, 122.0 (2C), 128.1, 128.6 (2C), 136.7, 157.8, 158.8, 159.0; HRMS (ESI), *m/z* calcd for $C_{14}H_{18}ClN_4O_3$ (MH^+) 325.1062, found 325.1060.

4.1.5. N^1-(4-Chlorophenyl)-N^2-(1-(phenylcarbamoyl)piperidin-4-yl)oxalamide (7)

To a stirred solution of **3** (140 mg, 0.498 mmol) in $CHCl_3$ (5.00 mL) was added phenyl isocyanate (54.0 μL, 0.500 mmol) and stirred at room temperature for 1 h. The precipitate was collected and washed with cold $CHCl_3$, and dried under reduced pressure to provide the title compound **7** as white powder. (64.1 mg, 32% yield).

^1H NMR (500 MHz, DMSO) δ 1.52–1.66 (m, 2H), 1.68–1.80 (m, 2H), 2.81–2.95 (m, 2H), 3.84–3.96 (m, 1H), 4.08–4.20 (m, 2H), 6.91–6.94 (m, 2H), 7.21–7.24 (m, 2H), 7.36–7.52 (m, 4H), 7.86 (d, J = 9.00 Hz, 2H), 8.53 (s, 1H), 8.99 (d, J = 8.50 Hz, 2H), 10.81 (s, 1H); ^{13}C NMR (125 MHz, DMSO) δ 31.3 (2C), 43.4 (2C), 47.5, 120.0 (2C), 122.0, 122.4 (2C), 128.6, 128.7 (2C), 129.1 (2C), 137.1, 141.1, 155.2, 159.2, 159.5; HRMS (ESI), *m/z* calcd for $C_{20}H_{22}ClN_4O_3$ (MH^+) 401.1375, found 401.1372.

4.1.6. N^1-(1-Benzoylpiperidin-4-yl)-N^2-(4-chlorophenyl) oxalamide (8)

To a stirred solution of **3** (500 mg, 1.78 mmol) in $CHCl_3$ (17.8 mL) was added benzoyl chloride (307 μL, 2.67 mmol) and the mixture was stirred at room temperature for 1 h. The precipitate was collected and washed with cold EtOAc, and dried under reduced pressure to provide the title compound **8** (232 mg, 34% yield).

^1H NMR (500 MHz, $CDCl_3$) δ 1.21–1.68 (br, 4H), 1.96–2.08 (br, 2H), 3.02–3.16 (br, 2H), 4.04–4.07 (m, 1H), 7.35 (d, J = 9.00 Hz, 2H), 7.41–7.43 (m, 5H), 7.52 (d, J = 8.00 Hz, 1H), 7.59 (d, J = 9.00 Hz, 2H), 9.25 (s, 1H); ^{13}C NMR (125 MHz, $CDCl_3$) δ 31.4 (2C), 41.0 (2C), 47.6, 121.0 (2C), 126.9 (2C), 128.6 (2C), 129.3 (2C), 129.9, 130.6, 134.8, 135.6, 157.2, 159.0, 170.5; HRMS (ESI), *m/z* calcd for $C_{20}H_{21}ClN_3O_3$ (MH^+) 386.1266, found 386.1276.

4.1.7. Amine (10)

To a stirred solution of 2,2,6,6-tetramethylpiperidin-4-one (7.75 g, 50.0 mmol) and cyclohexanone (15.5 mL, 150 mmol) in DMSO (71.0 mL) was added NH_4Cl (16.1 g, 300 mmol) and stirred at 60 °C for 5 h. The reaction mixture was diluted with H_2O

(150 mL), acidified with 7% aq HCl, and extracted with Et_2O (200 mL × 3). The water layer was adjusted to pH 9 using 10% aq K_2CO_3 and then back-extracted with EtOAc. The extract was washed with brine and dried over Na_2SO_4. After concentration under reduced pressure, the residue was dissolve in MeOH (60.0 mL) and benzylamine (10.9 mL, 100 mmol) was added. After being stirred at room temperature for 1 h, sodium cyanoborohydride was added and stirred at room temperature for 6 h. The reaction mixture was poured into saturated $NaHCO_3$ and extracted with EtOAc, then dried over $MgSO_4$. After concentration under reduced pressure, the residue was dissolve in MeOH (150 mL) and 10% Pd/C (5.32 g, 5.00 mmol) was added and stirred at room temperature for 24 h under hydrogen atmosphere. After the reaction mixture was filtered through celite, the filtrate solution was concentrated under reduced pressure followed by flash chromatography over silica gel with EtOAc–EtOH (4:1) to gave the title compound **10** (820 mg, 7 % yield) as a colorless oil.

^{1}H NMR (500 MHz, $CDCl_3$) δ 0.730 (t, J = 12.0 Hz, 2H), 1.15–1.85 (m, 23H), 2.01–3.7 (m, 2H), 2.95–3.05 (m, 1H); ^{13}C NMR (125 MHz, $CDCl_3$) δ 22.2 (2C), 22.8 (2C), 26.2 (2C), 37.3 (2C), 42.3 (2C), 43.6 (2C), 47.0, 53.2 (2C); HRMS (ESI), m/z calcd for $C_{15}H_{29}N_2$ (MH^+) 237.2325, found 237.2321.

4.1.8. N^1-(4-Chlorophenyl)-N^2-(2,6-dicyclohexylpiperidin-4-yl) oxalamide (11)

To a solution of **10** (722 mg, 3.05 mmol) in EtOH (15.0 mL) was added ethyl 2-((4-chlorophenyl)amino)-2-oxoacetate (363 mg, 1.50 mmol) and triethylamine (0.415 mL, 3.00 mmol) and stirred for 3 h at 150 °C under microwave irradiation. The mixture was filtered and the precipitate was collected and washed with cold EtOH, and dried under reduced pressure to provide the compound **11** (108 mg, 17% yield) as white powder.

^{1}H NMR (500 MHz, DMSO) δ 1.12–1.91 (br, 24H), 4.02–4.07 (m, 1H), 7.42 (d, J = 9.00 Hz, 2H), 7.84 (d, J = 9.00 Hz, 2H), 8.76 (br, 1H), 9.25 (s, 1H); ^{13}C NMR (125 MHz, $CDCl_3$) δ 22.1 (2C), 22.7 (2C), 26.0 (2C), 37.2 (2C), 42.5 (2C), 42.9 (2C), 43.6, 52.7 (2C), 120.9 (2C), 129.3 (2C), 130.4, 135.0, 157.6, 158.8; HRMS (ESI), m/z calcd for $C_{23}H_{33}ClN_3O_2$ (MH^+) 418.2256, found 418.2261.

4.1.9. N^1-(4-Chlorophenyl)-N^2-(4-fluorophenyl)oxalamide (14)

To a solution of the ethyl 2-((4-chlorophenyl)amino)-2-oxoacetate (1.21 g, 5.00 mmol) in EtOH (25.0 mL) were added Et_3N (1.38 mL, 10.0 mmol) and 4-fluoroaniline **12** (1.44 mL, 15.0 mmol). The reaction mixture was stirred for 3 h at 150 °C under microwave irradiation. After being cooled to room temperature, the crystal was collected and washed with cold EtOH and n-hexane, and dried under reduced pressure to provide the compound **14** (601 mg, 41% yield) as colorless crystals. Compounds **15** and **16** were similarly synthesized.

^{1}H NMR (500 MHz, $CDCl_3$) δ 7.07–7.14 (m, 2H), 7.35–7.40 (m, 2H), 7.59–7.63 (m, 4H), 9.29 (s, 1H), 9.33 (s, 1H); ^{13}C NMR (125 MHz, DMSO) δ 115.8 (d, J = 22.5 Hz, 2C), 122.5 (2C), 122.8 (d, J = 7.5 Hz, 2C), 128.8, 129.1 (2C), 134.4, 137.1, 158.3, 158.9 (d, J = 42.5 Hz), 160.2; HRMS (ESI), m/z calcd for $C_{14}H_{11}ClFN_2O_2$ (MH^+) 293.0488, found 293.0485.

4.1.10. N^1-(4-Chlorophenyl)-N^2-(2-(pyridin-2-yl)ethyl) oxalamide (17)

To a solution of the ethyl 2-((4-chlorophenyl)amino)-2-oxoacetate (726.3 mg, 3.00 mmol) in EtOH (10.0 mL) were added Et_3N (0.831 mL, 6.00 mmol) and 2-(pyridin-2-yl)ethanamine 14 (1.07 mL, 9.00 mmol). The reaction mixture was stirred for 3 h at 150 °C under microwave irradiation. After being cooled to room temperature, the crystal was collected and washed with cold EtOH and n-hexane, and dried under reduced pressure to provide the title compound **17** (336 mg, 37% yield) as colorless crystals.

^{1}H NMR (500 MHz, $CDCl_3$) δ 3.08 (t, J = 6.50 Hz, 2H), 3.82 (q, J = 6.50 Hz, 2H), 7.12–7.21 (m, 2H), 7.30–7.37 (m, 2H),7.54–7.66 (m 3H), 8.40 (s, 1H), 8.60 (d, J = 5.00 Hz, 1H), 9.26 (s, 1H); ^{13}C NMR (125 MHz, $CDCl_3$) δ 36.5, 39.0, 121.0 (2C), 121.8, 123.4, 129.2 (2C), 130.3, 135.1, 136.7, 149.5, 157.5, 158.6, 159.6; HRMS (ESI), m/z calcd for $C_{15}H_{15}ClN_3O_2$ (MH^+) 304.0847, found 304.0850.

4.2. Molecular modeling

The structures of compounds **11** and **12** were built in Sybyl and minimized with the MMFF94 force field and partial charges.[17] Dockings were then performed using FlexSIS through its SYBYL module, into the crystal structure of gp120 (PDB: 1RZJ).

4.3. FACS analysis

JR-FL (R5, Sub B) chronically infected PM1 cells were pre-incubated with 100 μM of a CD4 mimic for 15 min, and then incubated with an anti-HIV-1 mAb, 4C11, at 4 °C for 15 min. The cells were washed with PBS, and fluorescein isothiocyanate (FITC)-conjugated goat anti-human IgG antibody was used for antibody-staining. Flow cytometry data for the binding of 4C11 (green lines, Fig. 4) to the Env-expressing cell surface in the presence of a CD4 mimic are shown among gated PM1 cells along with a control antibody (anti-human CD19: black lines, Fig. 4). Data are representative of the results from a minimum of two independent experiments. The number at the bottom of each graph in Figure 4 shows the mean fluorescence intensity (MFI) of the antibody 4C11.

Acknowledgments

This work was supported in part by Grant-in-Aid for Scientific Research from the Ministry of Education, Culture, Sports, Science, and Technology of Japan, and Health and Labour Sciences Research Grants from Japanese Ministry of Health, Labor, and Welfare.

Supplementary data

Supplementary data (NMR charts of compounds) associated with this article can be found, in the online version, at doi:10.1016/j.bmc.2011.09.045.

References and notes

1. Selected reviews of the drug developments targeting HIV entry process: (a) Blair, W. S.; Lin, P. F.; Meanwell, N. A.; Wallace, O. B. *Drug Discovery Today* **2000**, *5*, 183; (b) D'Souza, M. P.; Cairns, J. S.; Plaeger, S. F. *J. Am. Med. Assoc.* **2000**, *284*, 215; (c) Labranche, C. C.; Galasso, G.; Moore, J. P.; Bolognesi, D.; Hirsch, M. S.; Hammer, S. M. *Antivir. Res.* **2001**, *50*, 95; (d) Pierson, T. C.; Doms, R. W. *Immunol. Lett.* **2003**, *85*, 113; (e) Tamamura, H.; Otaka, A.; Fujii, N. *Curr. HIV Res.* **2005**, *3*, 289.
2. Chan, D. C.; Kim, P. S. *Cell* **1998**, *93*, 681.
3. (a) Alkhatib, G.; Combadiere, C.; Broder, C. C.; Feng, Y.; Kennedy, P. E.; Murphy, P. M.; Berger, E. A. *Science* **1996**, *272*, 1955; (b) Choe, H.; Farzan, M.; Sun, Y.; Sullivan, N.; Rollins, B.; Ponath, P. D.; Wu, L.; Mackay, C. R.; LaRosa, G.; Newman, W.; Gerard, N.; Gerard, C.; Sodroski, J. *Cell* **1996**, *85*, 1135; (c) Deng, H. K.; Liu, R.; Ellmeier, W.; Choe, S.; Unutmaz, D.; Burkhart, M.; Marzio, P. D.; Marmon, S.; Sutton, R. E.; Hill, C. M.; Davis, C. B.; Peiper, S. C.; Schall, T. J.; Littman, D. R.; Landau, N. R. *Nature* **1996**, *381*, 661; (d) Doranz, B. J.; Rucker, J.; Yi, Y. J.; Smyth, R. J.; Samson, M.; Peiper, S. C.; Parmentier, M.; Collman, R. G.; Doms, R. W. *Cell* **1996**, *85*, 1149; (e) Dragic, T.; Litwin, V.; Allaway, G. P.; Martin, S. R.; Huang, Y.; Nagashima, K. A.; Cayanan, C.; Maddon, P. J.; Koup, R. A.; Moore, J. P.; Paxton, W. A. *Nature* **1996**, *381*, 667.
4. Feng, Y.; Broder, C. C.; Kennedy, P. E.; Berger, E. A. *Science* **1996**, *272*, 872.
5. (a) Briz, V.; Poveda, E.; Soriano, V. *J. Antimicrob. Chemother.* **2006**, *57*, 619; (b) Rusconi, S.; Scozzafava, A.; Mastrolorenzo, A.; Supuran, C. T. *Curr. Drug Targets Infect. Disord.* **2004**, *4*, 339; (c) Shaheen, F.; Collman, R. G. *Curr. Opin. Infect. Dis.* **2004**, *17*, 7; (d) Markovic, I. *Curr. Pharm. Des.* **2006**, *12*, 1105.
6. Zhao, Q.; Ma, L.; Jiang, S.; Lu, H.; Liu, S.; He, Y.; Strick, N.; Neamati, N.; Debnath, A. K. *Virology* **2005**, *339*, 213.
7. (a) Kwong, P. D.; Wyatt, R.; Robinson, J.; Sweet, R. W.; Sodroski, J.; Hendrickson, W. A. *Nature* **1998**, *393*, 648; (b) Kwong, P. D.; Wyatt, R.; Mcajeed, S.; Robinson, J.; Sweet, R. W.; Sodroski, J.; Hendrickson, W. A. *Structure* **2000**, *8*, 1329.

8. Schön, A.; Madani, N.; Klein, J. C.; Hubicki, A.; Ng, D.; Yang, X.; Smith, A. B., III; Sodroski, J.; Freire, E. *Biochemistry* **2006**, *45*, 10973.
9. Yoshimura, K.; Harada, S.; Shibata, J.; Hatada, M.; Yamada, Y.; Ochiai, C.; Tamamura, H.; Matsushita, S. *J. Virol.* **2010**, *84*, 7558.
10. Madani, N.; Schön, A.; Princiotto, A. M.; LaLonde, J. M.; Courter, J. R.; Soeta, T.; Ng, D.; Wang, L.; Brower, E. T.; Xiang, S.-H.; Do Kwon, Y.; Huang, C.-C.; Wyatt, R.; Kwong, P. D.; Freire, E.; Smith, A. B., III; Sodroski, J. *Structure* **2008**, *16*, 1689.
11. Yamada, Y.; Ochiai, C.; Yoshimura, K.; Tanaka, T.; Ohashi, N.; Narumi, T.; Nomura, W.; Harada, S.; Matsushita, S.; Tamamura, H. *Bioorg. Med. Chem. Lett.* **2010**, *20*, 354.
12. Narumi, T.; Ochiai, C.; Yoshimura, K.; Harada, S.; Tanaka, T.; Nomura, W.; Arai, H.; Ozaki, T.; Ohashi, N.; Matsushita, S.; Tamamura, H. *Bioorg. Med. Chem. Lett.* **2010**, *20*, 5853.
13. LaLonde, J. M.; Elban, M. A.; Courter, J. R.; Sugawara, A.; Soeta, T.; Madani, N.; Princiotto, A. M.; Kwon, Y. D.; Kwong, P. D.; Schön, A.; Freire, E.; Sodroski, J.; Smith, A. B., III *Bioorg. Med. Chem. Lett.* **2011**, *20*, 354.
14. Olofson, R. A.; Abbott, D. E. *J. Org. Chem.* **1984**, *49*, 2795.
15. Sakai, K.; Yamada, K.; Yamasaki, T.; Kinoshita, Y.; Mito, F.; Utsumi, H. *Tetrahedron* **2010**, *66*, 2311.
16. Bordwell, F. G.; Ji, G. Z. *J. Am. Chem. Soc.* **1991**, *113*, 8398.
17. Halgren, T. A. *J. Comput. Chem.* **1996**, *17*, 490.

ORIGINAL ARTICLE

CD70 Is Selectively Expressed on Th1 but Not on Th2 Cells and Is Required for Th1-Type Immune Responses

Tatsuyoshi Kawamura[1], Youichi Ogawa[1], Osamu Shimozato[2,4], Takashi Ando[3], Atsuhito Nakao[3], Tetsuji Kobata[2,5], Ko Okumura[2], Hideo Yagita[2] and Shinji Shimada[1]

The interaction between CD27 and CD70 provides a costimulatory signal for T-cell survival. Although the role of CD27 signaling in $CD8^+$ T cells has been well defined, its role in $CD4^+$ T cells is relatively unknown. Here, we report that CD70 is specifically expressed on differentiated T-helper (Th)1 cells, but not on Th2 cells. Upon activation, CD70 expression increased markedly on Th1 cells, but remained undetectable on Th2 cells. We demonstrate that CD27 is involved in naive T-cell expansion in Th1-type, but not in Th2-type, immune responses as *in vivo* treatment with anti-CD70 monoclonal antibody at induction resulted in a significant reduction of delayed-type and contact hypersensitivity responses, but not asthmatic responses. In both Th1-type responses, during the priming phase, CD70 was detected at earlier time points on dendritic cells (DCs) and at later time points on $CD4^+$ T cells. Our results indicate that CD70 may be useful as a marker to distinguish Th1 from Th2 cells. More importantly, CD27 function may be controlled by the differentially regulated kinetics of CD70 expression on DCs and $CD4^+$ T cells, and Th1 cell-specific CD70 expression may be involved in an amplification loop for polarized Th1-type immune responses through T cell–T cell interactions.

Journal of Investigative Dermatology advance online publication, 14 April 2011; doi:10.1038/jid.2011.36

INTRODUCTION

CD27 is expressed on thymocytes, as well as on naive $CD4^+$ and $CD8^+$ T cells (Borst *et al.*, 2005; Watts, 2005; Nolte *et al.*, 2009). Its unique ligand CD70 is transiently expressed on activated T cells, B cells, and dendritic cells (DCs), and CD27 function is controlled by a tightly regulated CD70 expression *in vivo* (Oshima *et al.*, 1998; Tesselaar *et al.*, 2003; Borst *et al.*, 2005; Bullock and Yagita, 2005; Watts, 2005; Sanchez *et al.*, 2007; Nolte *et al.*, 2009). CD27 provides a costimulatory signal for T cells by supporting the survival of activated T cells rather than by affecting cell division (Hendriks *et al.*, 2000, 2003; Borst *et al.*, 2005; Peperzak *et al.*, 2010). A number of studies have examined the costimulatory effect of CD27/CD70 signaling on $CD8^+$ T cells *in vivo* using viral infection, cardiac allograft, tumors rejection, and major histocompatibility complex class I-restricted delayed-type hypersensitivity (DTH) models, in which CD27 has a critical role for $CD8^+$ T cells in the accumulation of cytolytic effector cells and in memory formation (Borst *et al.*, 2005; Watts, 2005; Nolte *et al.*, 2009).

$CD4^+$ T cells can be divided into T-helper type 1 (Th1) and type 2 (Th2) cells according to distinct profiles of cytokine production (Abbas *et al.*, 1996; Ho and Glimcher, 2002). Th1 cells produce IFN-γ, whereas Th2 cells produce IL-4, IL-5, and IL-13. Several surface molecules have been shown to be differentially expressed between Th-cell subsets. For example, the IL-12 receptor β2 chain, IL-18R, chemokine receptors CXCR3 and CCR5, Tim-3, and natural killer group 2 molecules are preferentially or selectively expressed on Th1 cells, whereas the T1/ST2, CCR3, CCR4, and inducible T-cell co-stimulator molecules are mainly found on Th2 cells (Szabo *et al.*, 1997; D'Ambrosio *et al.*, 1998; Lohning *et al.*, 1998; Sallusto *et al.*, 1998; Xu *et al.*, 1998; McAdam *et al.*, 2000; Meyers *et al.*, 2002; Monney *et al.*, 2002).

The role of CD27/CD70 interactions in Th1 and Th2 cell-mediated immune responses is unclear. CD27−/− mice infected with the influenza virus showed impaired accumulation of both $CD4^+$ T and $CD8^+$ T cells in the lung and spleen, respectively (Hendriks *et al.*, 2000). However, no difference in the percentages of IFN-γ-producing $CD4^+$ T cells was observed between CD27−/− and CD27+/+ mice. Nevertheless, CD27−/− mice immunized with the intranasal ovalbumin (OVA) protein showed decreased frequency of IFN-γ- and IL-2-producing $CD4^+$ T cells (Xiao *et al.*, 2008). Similarly, B cell-specific CD70 transgenic mice showed marked increases in the number of $CD4^+$ T cells that produced more IFN-γ but similar levels of IL-2 and

[1]*Faculty of Medicine, Department of Dermatology, University of Yamanashi, Yamanashi, Japan;* [2]*Department of Immunology, Juntendo University School of Medicine, Tokyo, Japan and* [3]*Faculty of Medicine, Department of Immunology, University of Yamanashi, Yamanashi, Japan*

[4]*Current address: Division of Pathology, Chiba Cancer Center Research Institute, Chiba, Japan*

[5]*Current address: Department of Immunology, Dokkyo Medical University School of Medicine, Mibu, Tochigi, Japan*

Correspondence: Tatsuyoshi Kawamura, Faculty of Medicine, Department of Dermatology, University of Yamanashi, 1110 Shimokato, Chuo, Yamanashi 409-3898, Japan. E-mail: tkawa@yamanashi.ac.jp

Abbreviations: CFSE, carboxyfluorescein diacetate succinimidyl ester; CHS, contact hypersensitivity; DC, dendritic cell; DLN, draining lymph node; DNBS, 2,4-dinitrobenzene-sulfonic acid; DTH, delayed-type hypersensitivity; OVA, ovalbumin; PMA, phorbol 12-myristate 13-acetate

Received 27 July 2010; revised 8 December 2010; accepted 19 January 2011

tumor necrosis factor-α compared with wild-type mice (Arens *et al.*, 2001). In lymphocytic choriomeningitis virus infection, CD27 signaling in $CD4^+$ T cells enhanced the secretion of IFN-γ and tumor necrosis factor-α, leading to destruction of the splenic architecture (Matter *et al.*, 2006). Intriguingly, anti-CD70 mAb treatment significantly reduced the proinflammatory cytokines IL-6, tumor necrosis factor-α, and IFN-γ in an experimental inflammatory bowel disease model, whereas it did not affect tumor necrosis factor-α, IFN-γ, IL-4, IL-5, or IL-10 production in an experimental allergic conjunctivitis model (Sumi *et al.*, 2008; Manocha *et al.*, 2009). Thus, it is still unclear whether CD27/CD70 signaling is involved in $CD4^+$ T-cell priming, differentiation, or "polarization" *in vivo*.

In this study, we investigated the expression of CD70 on Th1 and Th2 cells derived from OVA-specific T-cell receptor transgenic mice, and the contribution of CD70 to OVA-specific Th1- and Th2-type immune responses *in vitro* and *in vivo*. We further investigated the role of CD27/CD70 signaling in contact hypersensitivity (CHS) by examining the effect of neutralizing anti-CD70 mAb *in vivo*.

RESULTS

Expression of CD27 and CD70 on Th1 and Th2 cells

We first examined the expression of CD27 and CD70 on activated Th1 and Th2 cells. Upon stimulation with ionomycin plus PMA (phorbol 12-myristate 13-acetate), Th1 and Th2 cell lines produced IFN-γ and IL-4, respectively (Figure 1a). CD27 was expressed on almost all resting Th1 and Th2 cells, but was partly downregulated by stimulation with immobilized anti-CD3 and anti-CD28 mAbs (Figure 1b). Stimulation of Th1 cells induced high CD70 expression levels that peaked at 48–72 hours and then gradually decreased. In contrast, no significant expression of CD70 was induced on Th2 cells by the same stimulation (Figure 1c). Similarly, although CD70 expression was not observed on resting or activated D10G4 cells, CD70 was expressed on activated 28-4 cells (Figure 1d). Furthermore, both resting and activated human Th1 cell line HK-12 cells expressed abundant CD70 (Supplementary Figure S1 online).

Engagement of CD27 increases the proliferation and cytokine production of naive $CD4^+$ T cells, but not of Th1 or Th2 cells

To examine the costimulatory function of CD27, naive $CD4^+$ T cells, Th1 and Th2 cell lines were stimulated with immobilized anti-CD3 mAb in the presence of coimmobilized anti-CD27 mAb or control IgG. Engagement of CD27 by anti-CD27 mAb significantly increased the proliferation and the IFN-γ and IL-4 production of naive $CD4^+$ T cells (Figure 2a), whereas it did not significantly affect the proliferation or cytokine production of Th1 or Th2 cells (Figure 2b). To further examine whether CD27/CD70 signaling is involved in T–T cell interactions, naive $CD4^+$ T cells or Th1 cells were stimulated with immobilized anti-CD3 and anti-CD28 mAb or with immobilized anti-CD3 mAb

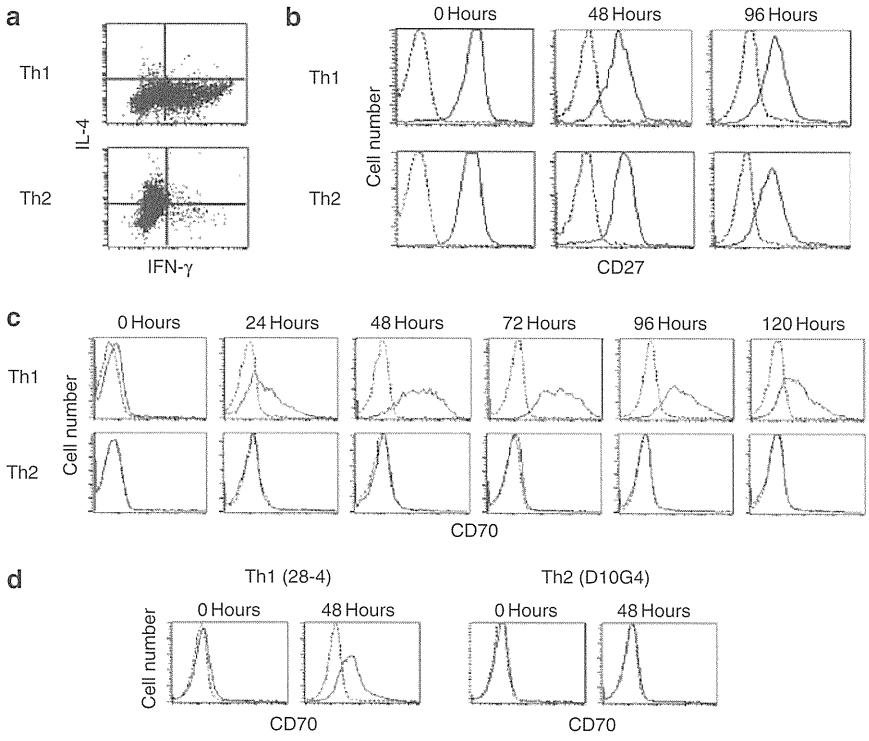

Figure 1. Expression of CD27 and CD70 on Th1 and Th2 cells. (**a**) Cytoplasmic staining for IFN-γ and IL-4. Th1 and Th2 cell lines were stimulated with PMA plus ionomycin for 24 hours. (**b**, **c**) Th1 and Th2 cell lines were stimulated with anti-CD3 and anti-CD28 mAbs for the indicated periods. Cells were stained with (**b**) anti-CD27 mAb or with (**c**) anti-CD70 mAb (solid lines). (**d**) Murine Th1 (28-4) and Th2 (D10G4) clones were stimulated with anti-CD3 and anti-CD28 mAbs for 48 hours, and then stained with anti-mouse or human CD70 mAb (solid lines). (**b**–**d**) Broken lines indicate background staining with control antibodies. All data are representative of three independent experiments with similar results. PMA, phorbol 12-myristate 13-acetate; Th, T-helper.

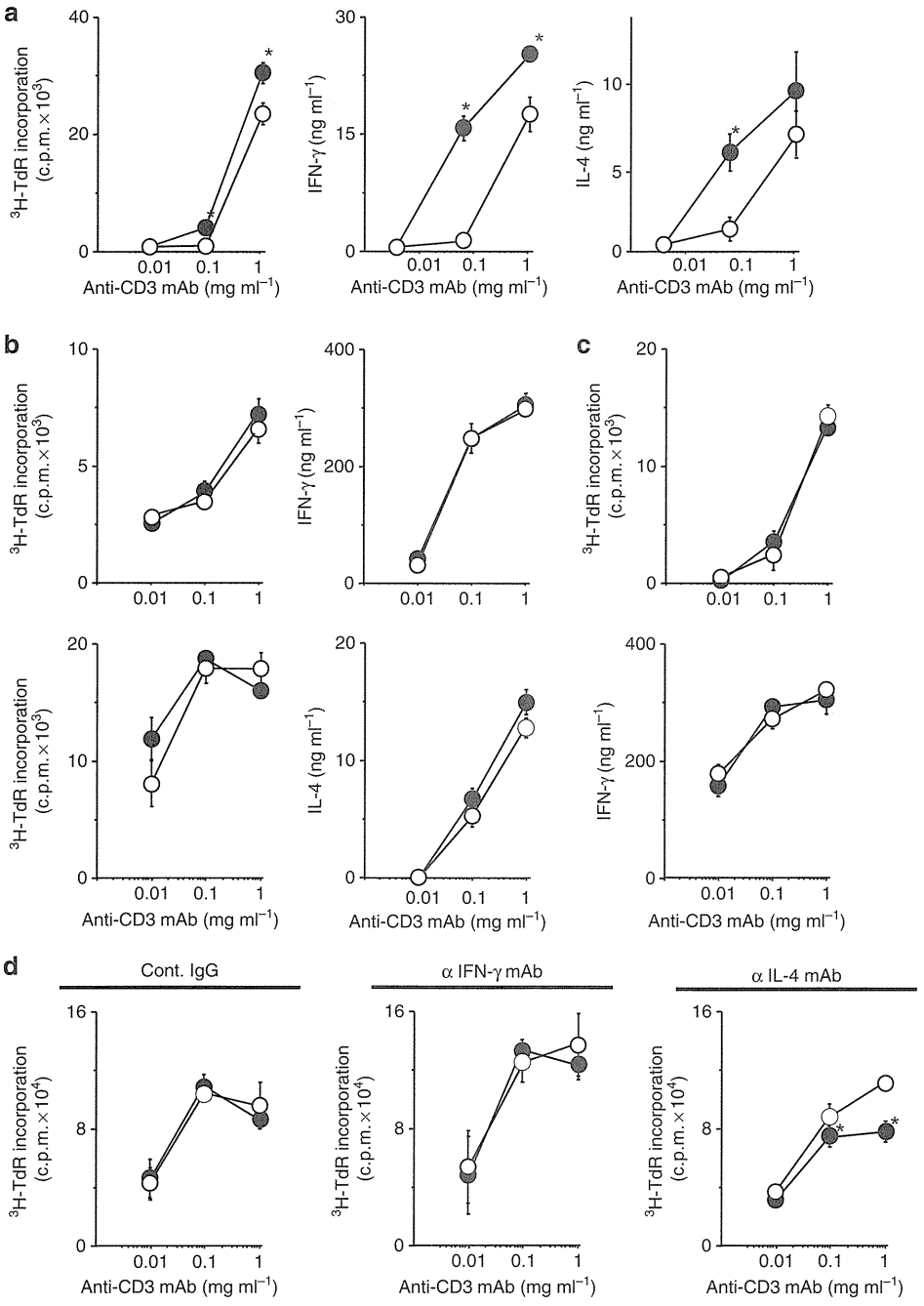

Figure 2. Engagement of CD27 increases the proliferation and cytokine production of naive CD4$^+$ T cells, but not of Th1 or Th2 cells. (**a**) Naive CD4$^+$ T cells, (**b**, upper panels) Th1, or (**b**, lower panels) Th2 cell lines were stimulated with anti-CD3 mAb in the presence of anti-CD27 mAb (●) or control IgG (○). (**c**) Th1 cell lines were stimulated with anti-CD3 mAb in the presence of anti-CD70 mAb (●) or control IgG (○). (**d**), Naive CD4$^+$ T cells were stimulated with anti-CD3 and anti-CD28 mAbs in the presence of the indicated mAbs and anti-CD70 mAb (●) or control IgG (○). Cells were assessed for proliferation and production of IFN-γ and/or IL-4. Similar results were obtained in three independent experiments. *$P<0.05$ compared with the control IgG group. Cont., control; Th, T-helper.

alone, respectively, in the presence of soluble anti-CD70 mAb or control IgG. Although we confirmed that CD70 was induced on naive CD4$^+$ T cells and Th1 cells by those stimulations (data not shown), no significant differences between control IgG and anti-CD70 mAb were observed in terms of naive CD4$^+$ T-cell proliferation (Figure 2d) or Th1-cell proliferation and IFN-γ production (Figure 2c). However, in the presence of anti-IL-4 mAb, anti-CD70 mAb significantly decreased naive CD4$^+$ T-cell expansion (Figure 2d), suggesting that IL-4 produced by activated T cells restricts T–T cell interaction by CD70/CD27 signaling.

CD70 is important for OVA-specific T-cell responses

To clarify the role of CD27/CD70 in CD4$^+$ T-cell responses *in vivo*, we used a DTH model (Kearney *et al.*, 1994).

DO11.10 (KJ1-26$^+$) CD4$^+$ T cells were adoptively transferred into BALB/c mice, and 2 days later, OVA/complete Freund's adjuvant (CFA) was injected subcutaneously (Kearney *et al.*, 1994). Intraperitoneal (i.p.) administration of anti-CD70 mAb significantly decreased the number of Ag-specific (KJ1-26$^+$) CD4$^+$ draining lymph node (DLN) T cells at day 6 compared with control Ig-treated mice (Figure 3a). When DO11.10 CD4$^+$ T cells were labeled with carboxyfluorescein diacetate succinimidyl ester (CFSE) before adoptive transfer, immunization with OVA/CFA dramatically induced cell division of KJ1-26$^+$ T cells, which was manifested by reduced CFSE levels (Figure 3b). Treatment with anti-CD70 mAb did not affect the cell division in KJ1-26$^+$ T cells (Figure 3b), whereas it significantly increased the percentage of apoptotic (annexin V$^+$) cells in KJ1-26$^+$ T cells as compared with control IgG-treated mice (Figure 3c). To explore the functional contribution of CD70 to cytokine production by KJ1-26$^+$ T cells, DLN cells were restimulated with the $OVA_{323–339}$ peptide *in vitro*. Strikingly, both the frequency of IFN-γ-secreting cells and the level of IFN-γ production were significantly reduced in cultures derived from anti-CD70 mAb-treated mice as compared with control IgG-treated mice (Figure 3d). These results suggest that the CD27/CD70 interaction has an important role in supporting Ag-specific naive CD4$^+$ T-cell expansion by allowing the primed CD4$^+$ T cells to survive successive divisions *in vivo*.

We next examined CD70 expression in this model. The number of CD70$^+$ KJ1-26$^+$ T cells and CD70 mRNA expression levels in CD4$^+$ T cells were dramatically increased after primary and secondary immunization with OVA/CFA (Figure 4a and b). Notably, CD70$^+$ cells were only detected in the CFSE^{low} KJ1-26$^+$ T-cell fraction, indicating that cell surface CD70 was expressed on activated T cells undergoing cell divisions. Interestingly, CD70 expression was observed on CD4$^+$ T cells 3 days after the first immunization, whereas its expression on CD11c$^+$ DCs peaked on day 1 (Figure 4c).

To confirm whether CD70 expressed on T cells is functional, CD4$^+$ T cells were purified from DLN cells harvested 3 days after immunization, and cultured in the presence of soluble anti-CD70 mAb or control IgG for 3 days. As expected, anti-CD70 mAb significantly decreased CD4$^+$ T-cell expansion (Figure 4d), suggesting that CD70 expressed on CD4$^+$ T cells is functional in T–T cell interaction.

CD70 is important for the induction of Th1-predominant CHS

To explore the role of CD27/CD70 in Th1-mediated diseases *in vivo*, we investigated DNFB-induced CHS. It has been

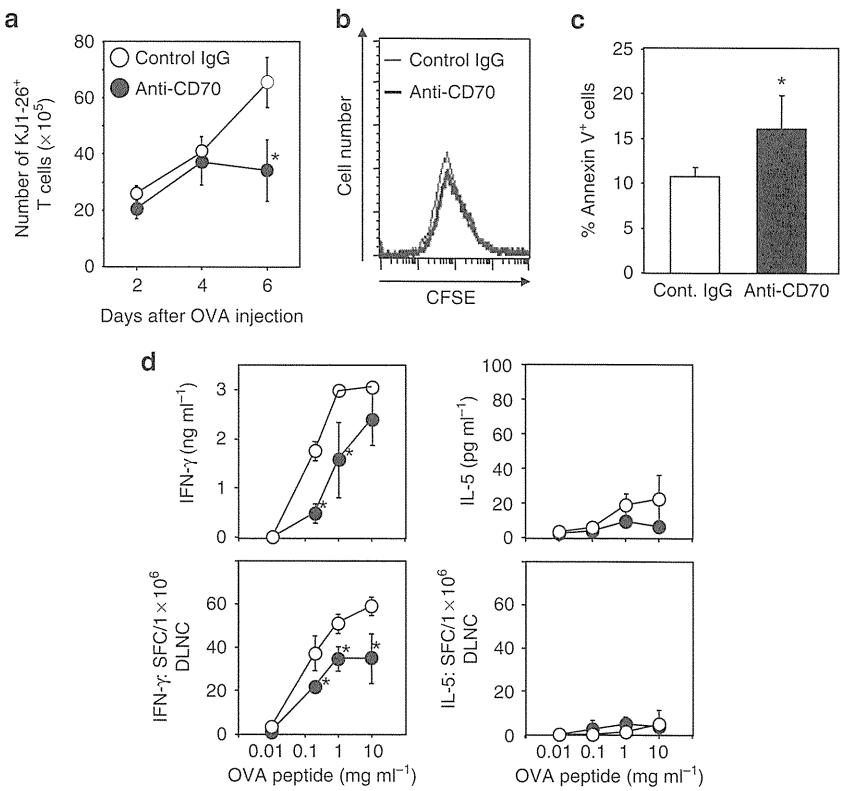

Figure 3. CD70 is important for naive T-cell survival in Th1 immune response. BALB/c recipients of DO11.10 T cells were immunized with OVA/CFA and administered with control IgG (○) or anti-CD70 mAb (●). DLNs were harvested at (**a**) the indicated time points or (**b–e**) 6 days after immunization. (**a**) The total number of KJ1-26$^+$ CD4$^+$ T cells in DLNs. (**b**) DO11.10 T cells were labeled with CFSE before adoptive transfer. Cell division of KJ1-26$^+$ CD4$^+$ T cells was compared by CFSE dilution. (**c**) Incidence of apoptosis in KJ1-26$^+$ DLN cells as determined by annexin V binding. (**d**) DLN cells were restimulated with the $OVA_{323–339}$ peptide and assessed for cytokine production by ELISA (upper panels) and ELISPOT (lower panels). Similar results were obtained in three independent experiments. *$P<0.05$ compared with the control IgG group. Cont., control; CFSE, carboxyfluorescein diacetate succinimidyl ester; DLN, draining lymph node; OVA, ovalbumin; SFC, spot-forming cells; Th, T-helper.

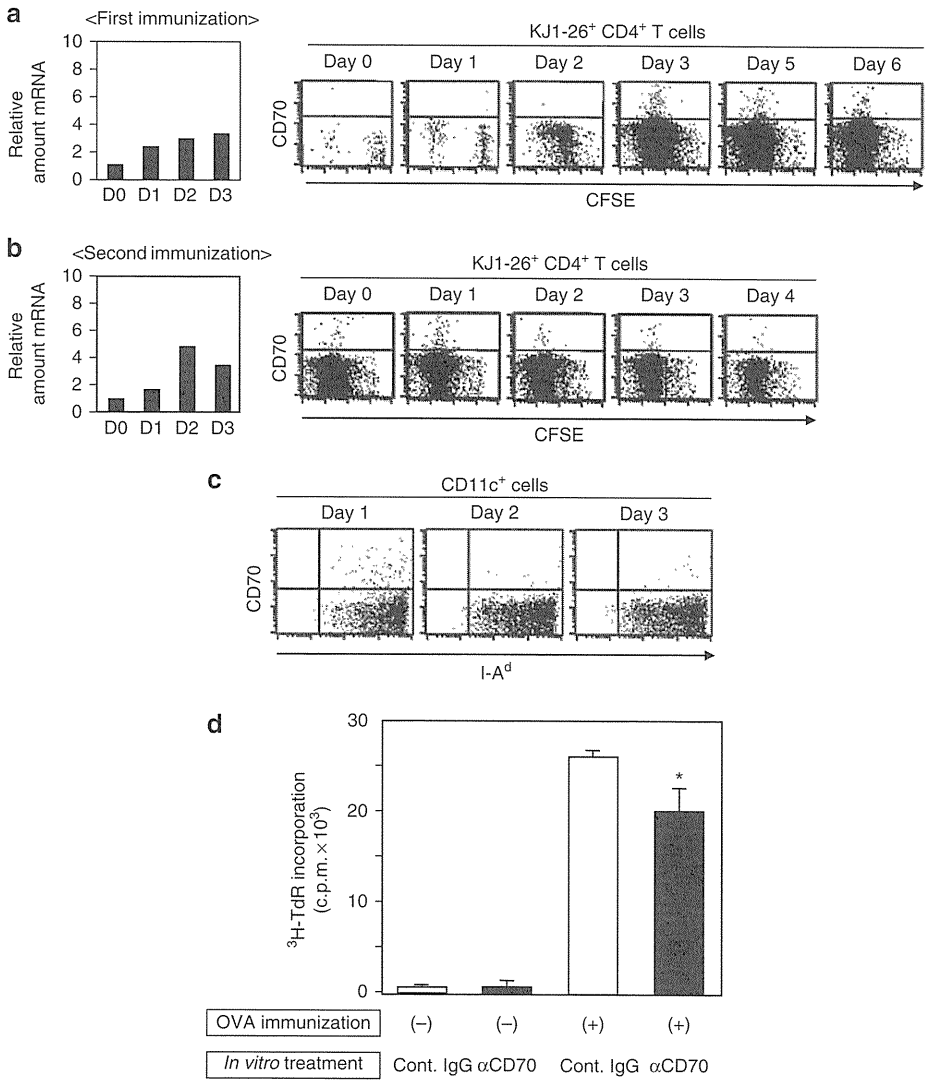

Figure 4. CD70 expression *in vivo*. BALB/c recipients of DO11.10 $CD4^+$ T cells were immunized with OVA/CFA (**a**, **c**, **d**) or re-immunized 7 days after the first immunization (**b**), and DLN cells were harvested at the indicated time points. (**a** and **b**, upper panels) Real-time PCR quantification of CD70 mRNA. For purified $CD4^+$ T cells isolated from DLNs, CD70 mRNA copy numbers were normalized to G3PDH mRNA. Results are presented as fold induction over baseline values obtained at day 0. (**a** and **b** lower panels) DO11.10 $CD4^+$ T cells were labeled with CFSE before adoptive transfer. Data show CD70 expression on electronically gated $CD4^+$ KJ1-26^+ DLN cells. (**c**) DLN cells were harvested at the indicated time points. Data show CD70 expression on electronically gated $CD11c^+$ cells. (**d**) $CD4^+$ T cells were purified from DLN cells harvested 3 days after immunization. Cells were cultured in the presence of anti-CD70 mAb (black bar) or control IgG (white bar) for 3 days, and assessed for proliferation. Similar results were obtained in three independent experiments. CFSE, carboxyfluorescein diacetate succinimidyl ester; Cont., control; DLN, draining lymph node; OVA, ovalbumin.

shown using CD8−/− and CD4−/− mice that both $CD4^+$ Th1 and $CD8^+$ T cells are crucial effector cells in CHS responses to DNFB (Wang *et al.*, 2000). Interestingly, treatment with anti-CD70 mAb at sensitization significantly inhibited ear swelling as compared with control Ig-treated mice (Figure 5a), whereas treatment at challenge did not significantly affect ear swelling (Figure 5b). DLN cells isolated 5 days after DNFB sensitization produced a high level of IFN-γ and a low level of IL-4 in response to DNBS (2,4-dinitrobenzene-sulfonic acid, a water-soluble analog of DNFB) restimulation (Figure 5c). The frequency of IFN-γ-secreting cells and the level of IFN-γ production were significantly reduced in cultures derived from mice treated with anti-CD70 mAb as than in those from control IgG-treated mice (Figure 5c and d). In contrast, the *in vitro* addition of anti-CD70 mAb during DNBS restimulation did not significantly affect the frequency of IFN-γ-producing cells recovered from DNFB-sensitized mice (Figure 5d). A small population of $CD4^+$ T cells and $CD8^+$ T cells isolated from DLNs expressed CD70 (Figure 5e), and CD70 mRNA was also induced in $CD11c^+$ DCs in DLNs after sensitization (Figure 5f). Notably, we could not detect significant CD70 expression on Th2, Th17, or regulatory T cells isolated from DLNs (Supplementary Figure S2 online). These findings

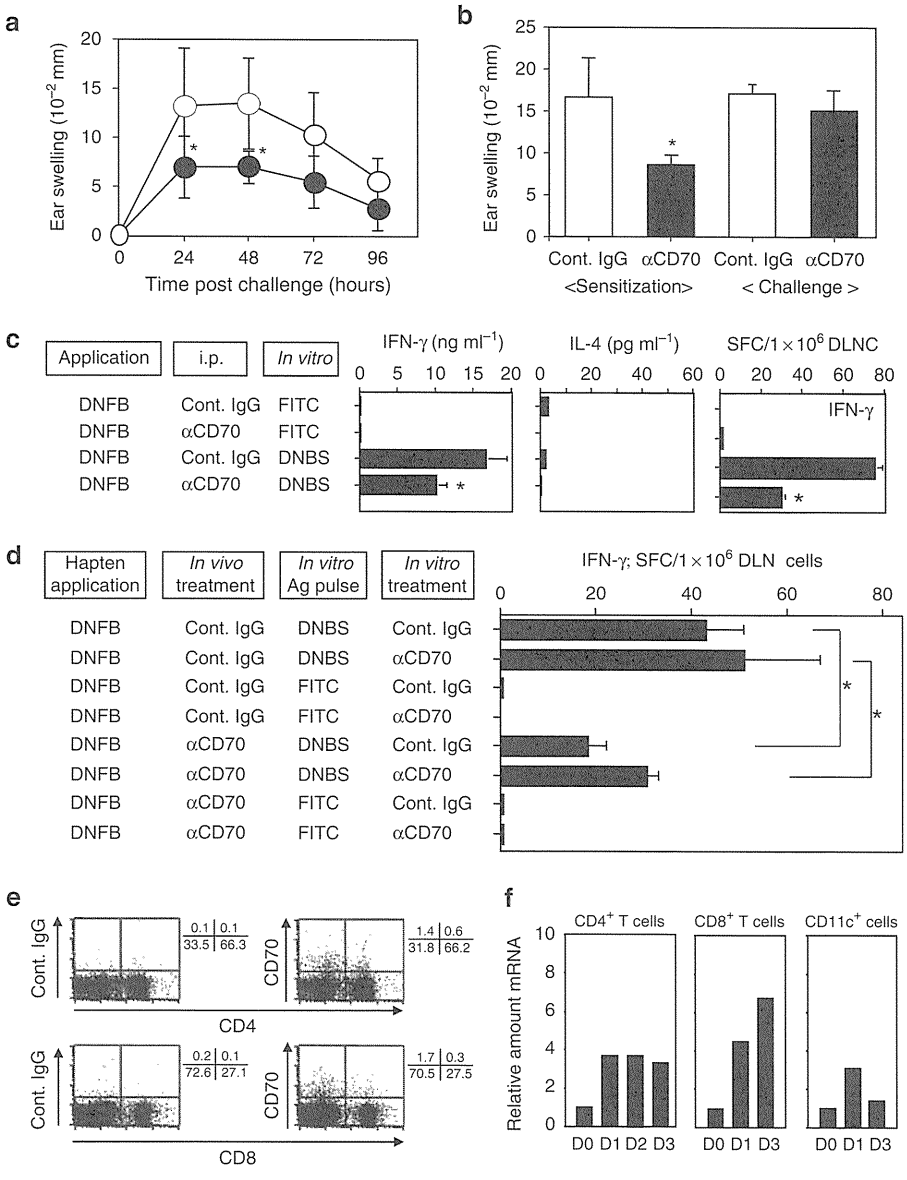

Figure 5. Administration of anti-CD70 mAb at sensitization inhibits CHS. CHS against DNFB was induced. Control IgG or anti-CD70 mAb was injected intraperitoneally (**a–d**) 2 hours before and 2 days after sensitization or (**b**) 2 hours before challenge. Ear thickness was evaluated at the (**a**) indicated time points or (**b**) 24 hours after challenge. (**c** and **d**) DNBS- or FITC-pulsed DLN cells from each group of mice were cultured and assessed for cytokine production. (**d**) Cells were cultured in the presence of anti-CD70 mAb or control IgG. **(e)** Data show CD70 expression on electronically gated CD3$^+$ DLN cells. (**f**) Real-time PCR quantification of CD70 mRNA for indicated cells purified from DLNs. Results are presented as fold induction over baseline values of each cell type obtained at day 0. *$P<0.05$ compared with the control IgG group. Data are representative of several experiments with similar results. CHS, contact hypersensitivity; Cont., control; DLN, draining lymph node; i.p., intraperitoneal; SFC, spot-forming cells.

suggested that CD27/CD70 signaling may support Ag-specific primed T-cell expansion during the sensitization phase of the CHS response.

Blockade of the CD70/CD27 interaction did not affect Th2-mediated asthmatic responses

To clarify the role of CD27/CD70 in Th2-type immune responses *in vivo*, we used a murine model of asthma caused by allergen-specific Th2 cells (Wills-Karp, 1999). As shown in Figure 6a–c, administration of anti-CD70 mAb did not significantly affect the serum anti-OVA IgE and IgG1 levels, Th2 cytokine levels in bronchoalveolar lavage fluid, and inflammatory cell infiltration around the bronchioles, as compared with those in control IgG-treated mice. In addition, when splenic T cells were restimulated with OVA *in vitro*, the production of IFN-γ, IL-4, and IL-5 was not significantly inhibited in anti-CD70 mAb-treated mice (Figure 6d). These results indicate that unlike Th1 responses, the blockade of CD70 during the induction phase did not affect the development of asthmatic Th2 responses. Consistent with these findings, we could not detect significant CD70 expression on CD4$^+$ cells obtained from DLNs and splenic cells after last immunization with OVA in asthmatic responses (Figure 6e and f).

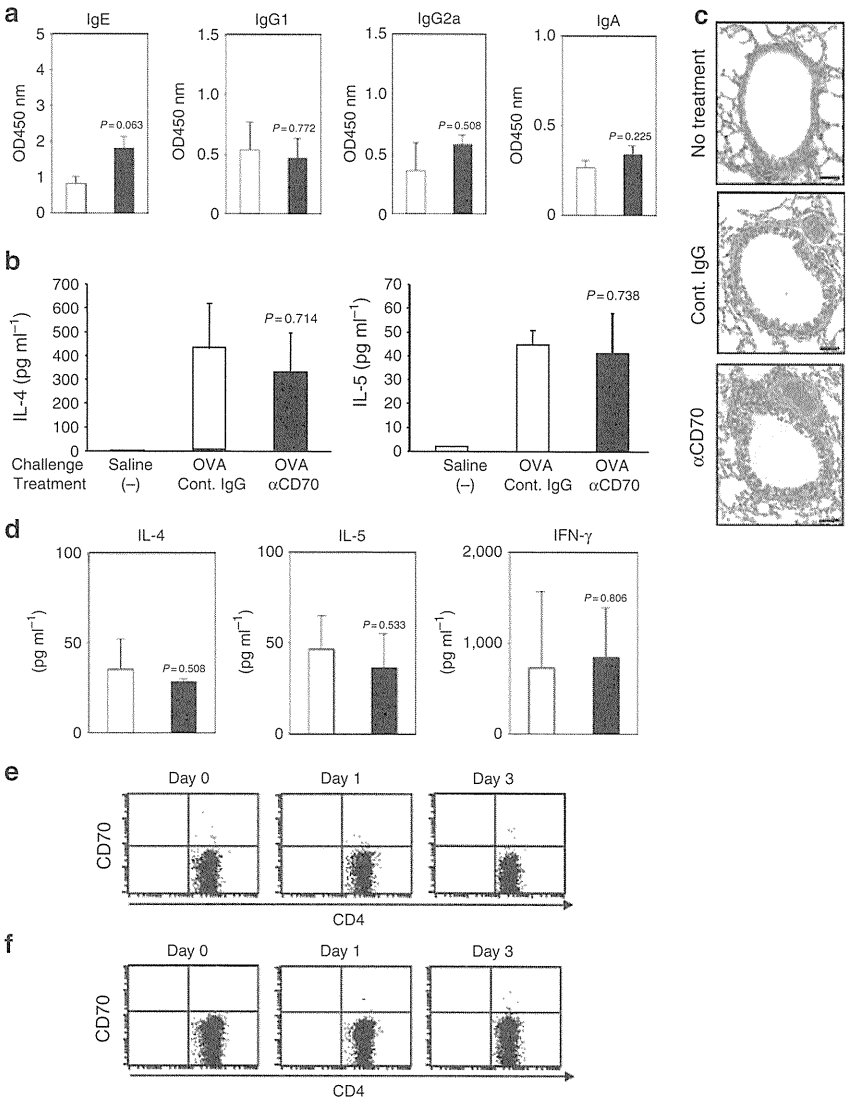

Figure 6. Administration of anti-CD70 mAb at sensitization does not affect asthmatic responses. BALB/c mice were immunized with OVA/alum on days 0 and 12, and then challenged with saline or OVA on days 22, 23, and 24. Control IgG or anti-CD70 mAb was injected intraperitoneally every 3 days from day 0 to day 18. (**a**) Twenty-four hours after the last OVA challenge, OVA-specific IgE, IgG1, IgG2a, and IgA serum antibody levels were determined by ELISA. (**b**) Cytokine levels in the BALF were measured by ELISA. (**c**) Histological examination of the lungs by H–E staining. Scale bar = 2 μm. (**d**) Splenocytes from sensitized mice treated with either control IgG or anti-CD70 mAb were stimulated with OVA *in vitro*. Cytokine levels in the supernatants were measured by ELISA. *P*-value: compared with the control IgG group. (**e**, **f**) DLN (**e**) and splenic (**f**) cells obtained 0, 1, and 3 days after the last immunization were stained with anti-CD70 and anti-CD4 mAb. Data showing the staining of electronically gated $CD4^+$ T cells. Data are representative of several experiments with similar results. alum, aluminum hydroxide; BALF, bronchoalveolar lavage fluid; Cont., control; DLN, draining lymph node; H–E, hematoxylin and eosin; OVA, ovalbumin.

DISCUSSION

We demonstrated that *in vivo* blockade of CD70/CD27 signaling significantly inhibited antigen-specific naive $CD4^+$ T-cell expansion and Th1-cell generation, and increased the number of apoptotic cells in Ag-specific T cells without affecting cell division (Figure 3). However, we found that CD27/CD70 signaling was not critically involved in either [^{3}H]-thymidine incorporation or cytokine production by Th1 or Th2 cells (Figure 2). These findings suggest that CD27 signaling may be required for survival of primed T cells, but not of polarized Th1 or Th2 cells, and have a critical role in supporting the survival of Ag-primed T cells during the induction phase of Th1-type immune responses. This notion is supported by the fact that inhibitory effects of anti-CD70 mAb were only observed during the sensitization, but not the challenge, phase of the Th1- and Tc1-mediated CHS response.

We found that during the DTH response, CD70 expression on $CD4^+$ T cells was observed 3–6 days after the first immunization, whereas CD70 expression on DCs peaked at 1 day after immunization (Figure 4). Similarly, during the CHS response, abundant CD70 mRNA expression was observed in T cells at 3 days after sensitization, whereas its expression rapidly decreased in $CD11c^+$ DCs/Langerhans cells at day 3 (Figure 5). As it has been reported for both

responses that Ag-bearing DCs and Langerhans cells rapidly disappear from the DLN 48–72 hours after immunization (Ingulli *et al.*, 1997; Kawamura *et al.*, 1999), it is possible that the rapid loss of CD70 on DCs/Langerhans cells, probably induced by interaction with CD40L-expressing $CD4^+$ T cells (Taraban *et al.*, 2004; French *et al.*, 2007), may be due to the disappearance of these cells from the DLN. In humans, a direct cellular communication between $CD45RO^+$ and $CD45RA^+$ T cells through CD27/CD70 has been proposed (Agematsu *et al.*, 1995). It is possible that CD70 expressed on Th1 cells contributes to an amplification loop of polarized Th1-type immune responses through Th1 cell-naive T-cell interactions. Indeed, we found that in the absence of IL-4, blockade of CD27/CD70 signaling through T–T cell interaction significantly decreased naive $CD4^+$ T-cell expansion (Figure 2d). Taken together, the above findings suggest that the CD27 function is controlled by the differentially regulated kinetics of CD70 expression on DCs and activated $CD4^+$ T cells during the priming phase of Th1 immune responses *in vivo*. It has been demonstrated that administration of the recombinant soluble CD70 protein during antigen stimulation resulted in a massive expansion of Ag-specific $CD8^+$ T cells *in vivo* (Rowley and Al-Shamkhani, 2004). Moreover, T cell-specific CD70 transgenic mice infected with the influenza virus showed enhanced numbers of effector memory $CD4^+$ T cells in B-cell follicles (Beishuizen *et al.*, 2009), thus suggesting that like studies in humans (Agematsu *et al.*, 1995), CD70 expressed on T cells is functional and provides CD27 signaling in activating $CD4^+$ T cells *in vivo*. Nevertheless, these mice in steady state did not show enhanced effector memory formation of $CD4^+$ T cells, despite the fact that the expression of Ki-67 was upregulated in effector memory $CD4^+$ T cells (van Gisbergen *et al.*, 2009). Although we demonstrated that CD70 expressed on $CD4^+$ T cells is functional in T–T cell interaction (Figures 2d and 4d), further studies are required to determine the functional significance of CD70 on $CD4^+$ T cells *in vivo*.

In this study, we have shown that blockade of the CD70/CD27 interaction inhibits Th1-mediated DTH and CHS responses, but does not affect Th2-mediated asthmatic responses. We also found that CD70 is expressed on Th1, but not on Th2, cells and clones, and that IL-4 strongly suppressed induction of CD70 expression on $CD4^+$ T cells (Figure 1 and data not shown). In addition, we could detect *ex vivo* CD70 expression on $CD4^+$ cells in Th1-mediated DTH and CHS, but not in Th2-mediated asthmatic responses (Figures 4, 5 and 6). In this regard, it has been demonstrated that induction of CD70 expression on human monocyte-derived DCs by lipopolysaccharide required an absence of IL-4 (Iwamoto *et al.*, 2005). On the other hand, CD70 on splenic $DEC\text{-}205^+$ DCs is important for the induction of IL-12-independent IFN-γ production by $CD4^+$ T cells *in vivo* (Soares *et al.*, 2007), and in the presence of IL-12, CD27 signaling promotes Th1 development *in vitro* (van Oosterwijk *et al.*, 2007). Nevertheless, human CD70 expressed on DCs promotes the development of $CD4^+$ T cells that produce both Th1 and Th2 cytokines (Hashimoto-Okada *et al.*, 2009). One possible explanation for the above findings is that IL-4 produced by $CD4^+$ T cells critically restricts CD70 expression on both DCs and $CD4^+$ T cells in type 2 immune responses *in vivo*, and therefore only in the setting of IL-4 paucity (e.g., Th1-type immune responses), CD70/CD27-mediated DC-T cell or T–T cell interactions have a role in activating naive $CD4^+$ T cells. This idea may, at least in part, account for the discordant results in previous reports regarding *in vivo* roles of the CD70/CD27 interaction in various $CD4^+$ T cell-mediated disease models, including inflammatory bowel disease (Sumi *et al.*, 2008) and experimental allergic conjunctivitis (Manocha *et al.*, 2009) models.

MATERIALS AND METHODS

Animals

Six-week-old female BALB/c and DO11.10 mice were purchased from Charles River Japan (Atsugi, Japan) and the Jackson Laboratory (Bar Harbor, ME), respectively. All mice were used in accordance with the guidelines of the Committee on Animals of Juntendo University and the University of Yamanashi.

Reagents and antibodies

Ovalbumin, lipopolysaccharide, PMA, ionomycin, and CFA were purchased from Sigma (St Louis, MO). The cell-permeant fluorescent dye CFSE was purchased from Molecular Probes (Eugene, OR). An anti-murine CD70 mAb (FR70, rat IgG2b) was prepared as described previously (Oshima *et al.*, 1998). The other mAbs were purchased from BD Pharmingen (San Jose, CA).

Cell lines and tissue culture

Th1 and Th2 cell lines were originated from naive $CD4^+$ T cells prepared from the spleen or lymph node of OVA-specific TCR-αβ transgenic mice (DO11.10) as described previously (Watanabe *et al.*, 1997). T-cell clones used were: HK-12 (human Th1 clone derived from phytohemagglutinin-stimulated peripheral blood lymphocyte), 28-4 (murine Th1 clone specific for KLH), and D10G4 (murine Th2 clone, specific for conalbumin). T-cell lines and clones were maintained in RPMI 1640 medium containing 10% fetal calf serum, 10 mM HEPES, 0.25 μg ml^{-1} gentamycine, 2 mM L-glutamine (complete medium), and 50 Units ml^{-1} recombinant human IL-2 (Shionogi, Osaka, Japan). Naive T cells, T-cell lines, and clones were stimulated with immobilized anti-CD3 mAb (0.01–10 μg ml^{-1}) in the presence or absence of immobilized control IgG or mAbs (10 μg ml^{-1}) against CD28 and CD27 or with PMA (50 ng ml^{-1}) plus ionomycin (500 ng ml^{-1}).

OVA-specific DTH responses and mAb treatment *in vivo*

DO11.10 T cells were identified by staining with KJ1-26 mAb (Caltag, Burlingame, CA) and prepared for adoptive transfer as described previously (Kearney *et al.*, 1994). In brief, transgenic lymph nodes and spleen cells depleted of $CD8^+$ T cells were adoptively transferred by intravenous injection into BALB/c mice such that 2×10^6 $KJ1\text{-}26^+$ T cells were given to each recipient. Mice were injected subcutaneously with 100 μg OVA emulsified in CFA (upper and lower back) 2 days later. Groups of five mice received i.p. injection of 250 μg per mouse anti-CD70 mAb or control IgG 2 hours before and 48 hours after immunization. In some experiments, DO11.10 T cells were stained with 2.5 μM CFSE before adoptive transfer. To determine cytokine production, 4×10^6 DLN

cells collected 6 days after immunization were cultured in the presence of 0–10 μg ml^{-1} $OVA_{323–339}$ peptide for 48 hours.

Contact hypersensitivity

A volume of 20 μl of 0.5% DNFB dissolved in acetone:olive oil (4:1) was painted on the shaved abdomen of mice at days 0 and 1, and then the ears of mice were challenged with 10 μl of 0.2% DNFB on day 5. Ear thickness was measured as described previously (Nuriya *et al.*, 2001). Groups of five mice received i.p. injection of 250 μg per mouse anti-CD70 mAb or control IgG 2 hours before and 48 hours after sensitization or 2 hours before challenge. To determine cytokine production, DLN cells collected from mice 5 days after sensitization or challenge were incubated with 10 mM DNBS (Tokyo Kasei, Tokyo, Japan) or 0.3 mg ml^{-1} FITC (isomer-I, Dojindo, Kumamoto, Japan) for 10 minutes as described previously (Nuriya *et al.*, 2001).

Induction of allergic airway inflammation and mAb treatment *in vivo*

Groups of five mice were sensitized by i.p. injection of 50 μg OVA with 1 mg aluminum hydroxide (alum) on days 0 and 12. On days 22, 23, and 24, mice received intranasal challenges of either 20 μl of saline or 20 μl of saline containing 100 μg of OVA. Twenty-four hours after the last OVA challenge, the trachea was cannulated with a polyethylene tube through which the lungs were gently lavaged with 0.8 ml phosphate-buffered saline containing 0.1% BSA three times (2.4 ml total of bronchoalveolar lavage fluid). On day 25, OVA-specific IgE, IgG1, IgG2a, and IgA serum antibody levels were determined by ELISA (Hoshino *et al.*, 2003). The lungs were removed from mice 24 hours after the last OVA challenge, fixed in 10% neutral-buffered formalin, and embedded in paraffin. Sections of 5-μm thickness were stained with hematoxylin and eosin. To determine cytokine production, splenocytes collected on day 25 were incubated with OVA (100 μg ml^{-1}) for 72 hours. To examine the effect of anti-CD70 mAb, mice were i.p. injected with 300 μg of anti-CD70 mAb or control IgG every 3 days from day 0 to day 18.

Real-time PCR

$CD4^+$ T cells, $CD8^+$ T cells, and DCs were positively selected from DLN cells using anti-CD4, anti-CD8, and anti-CD11c magnetic beads, respectively, and MACS columns (Militenyi Biotec, San Diego, CA). Relative CD70 mRNA expression was determined by real-time PCR using an ABI PRISM 5500 Sequence Detection System (Applied Biosystems, Framingham, MA) with SYBR Green I dye (Qiagen, Tokyo, Japan). Total RNA was isolated using TRIzol (Invitrogen Life Technologies, Carlsbad, CA), and cDNA was synthesized using the SuperScript system (Invitrogen Life Technologies). Primers corresponding to mouse CD70 and G3PDH were designed by Takara Bio (Shiga, Japan) as follows: 5′-AGCGGACTACTCAGTAAGCAGCAAC-3′ and 5′-CAGCTCTGGTCCGTGTGTGAA-3′ for CD70, and 5′-AAATGGTGAAGGTCGGTGTG-3′ and 5′-TGAAGGGGTCGTTGATGG-3′ for G3PDH. Cycle threshold numbers (Ct) were derived from the exponential phase of PCR amplification. Fold differences in the expression of gene x in the cell populations y and z were derived by 2^k, where $k=(Ctx-Ct_{G3PDH})y-(Ctx-Ct_{G3PDH})z$.

Flow cytometry

Cells (5×10^5) were stained with the indicated mAbs (10 μg ml^{-1}) for 30 minutes at 4°C and analyzed on a FACSCalibur (Becton Dickinson, San Jose, CA). FITC-labeled annexin V (R&D Systems, Minneapolis, MN) was used for detection of apoptosis. To assess intracellular cytokine production, cells were surface stained, fixed and permeabilized, and then stained intracellularly for IFN-γ, IL-4, and IL-17.

In vitro proliferation and cytokine assays

Naive CD4 T cells, Th1, and Th2 cells stimulated as described above were cultured for 72–96 hours and the proliferative response was measured by [^{3}H]-thymidine (^{3}H-TdR) uptake (0.5 μCi per well) for the last 16 hours. Cell-free culture supernatants and cells were assayed using cytokine-specific ELISA and ELISPOT assay kits, respectively (R&D Systems).

Statistical analyses

Significant differences between experimental groups were analyzed by Student's *t*-test. *P*-values <0.05 were considered significant.

CONFLICT OF INTEREST

The authors state no conflict of interest.

ACKNOWLEDGMENTS

We thank Naotaka Shibagaki and Hiroyuki Matsue for helpful discussions, and Izumi Ishikawa for technical assistance.

SUPPLEMENTARY MATERIAL

Supplementary material is linked to the online version of the paper at http://www.nature.com/jid

REFERENCES

Abbas AK, Murphy KM, Sher A (1996) Functional diversity of helper T lymphocytes. *Nature* 383:787–93

Agematsu K, Kobata T, Sugita K *et al.* (1995) Direct cellular communications between CD45R0 and CD45RA T cell subsets via CD27/CD70. *J Immunol* 154:3627–35

Arens R, Tesselaar K, Baars PA *et al.* (2001) Constitutive CD27/CD70 interaction induces expansion of effector-type T cells and results in IFNgamma-mediated B cell depletion. *Immunity* 15:801–12

Beishuizen CR, Kragten NA, Boon L *et al.* (2009) Chronic CD70-driven costimulation impairs IgG responses by instructing T cells to inhibit germinal center B cell formation through FasL-Fas interactions. *J Immunol* 183:6442–51

Borst J, Hendriks J, Xiao Y (2005) CD27 and CD70 in T cell and B cell activation. *Curr Opin Immunol* 17:275–81

Bullock TN, Yagita H (2005) Induction of CD70 on dendritic cells through CD40 or TLR stimulation contributes to the development of CD8+ T cell responses in the absence of CD4+ T cells. *J Immunol* 174:710–7

D'Ambrosio D, Iellem A, Bonecchi R *et al.* (1998) Selective up-regulation of chemokine receptors CCR4 and CCR8 upon activation of polarized human type 2 Th cells. *J Immunol* 161:5111–5

French RR, Taraban VY, Crowther GR *et al.* (2007) Eradication of lymphoma by CD8 T cells following anti-CD40 monoclonal antibody therapy is critically dependent on CD27 costimulation. *Blood* 109:4810–5

Hashimoto-Okada M, Kitawaki T, Kadowaki N *et al.* (2009) The CD70-CD27 interaction during the stimulation with dendritic cells promotes naive CD4(+) T cells to develop into T cells producing a broad array of immunostimulatory cytokines in humans. *Int Immunol* 21:891–904

Hendriks J, Gravestein LA, Tesselaar K *et al.* (2000) CD27 is required for generation and long-term maintenance of T cell immunity. *Nat Immunol* 1:433–40

Hendriks J, Xiao Y, Borst J (2003) CD27 promotes survival of activated T cells and complements CD28 in generation and establishment of the effector T cell pool. *J Exp Med* 198:1369–80

Ho IC, Glimcher LH (2002) Transcription: tantalizing times for T cells. *Cell* 109(Suppl):S109–20

Hoshino A, Tanaka Y, Akiba H *et al.* (2003) Critical role for OX40 ligand in the development of pathogenic Th2 cells in a murine model of asthma. *Eur J Immunol* 33:861–9

Ingulli E, Mondino A, Khoruts A *et al.* (1997) *In vivo* detection of dendritic cell antigen presentation to CD4(+) T cells. *J Exp Med* 185:2133–41

Iwamoto S, Ishida M, Takahashi K *et al.* (2005) Lipopolysaccharide stimulation converts vigorously washed dendritic cells (DCs) to nonexhausted DCs expressing CD70 and evoking long-lasting type 1 T cell responses. *J Leukoc Biol* 78:383–92

Kawamura T, Azuma M, Kayagaki N *et al.* (1999) Fas/Fas ligand-mediated elimination of antigen-bearing Langerhans cells in draining lymph nodes. *Br J Dermatol* 141:201–5

Kearney ER, Pape KA, Loh DY *et al.* (1994) Visualization of peptide-specific T cell immunity and peripheral tolerance induction *in vivo*. *Immunity* 1:327–39

Lohning M, Stroehmann A, Coyle AJ *et al.* (1998) T1/ST2 is preferentially expressed on murine Th2 cells, independent of interleukin 4, interleukin 5, and interleukin 10, and important for Th2 effector function. *Proc Natl Acad Sci USA* 95:6930–5

Manocha M, Rietdijk S, Laouar A *et al.* (2009) Blocking CD27-CD70 costimulatory pathway suppresses experimental colitis. *J Immunol* 183:270–6

Matter M, Odermatt B, Yagita H *et al.* (2006) Elimination of chronic viral infection by blocking CD27 signaling. *J Exp Med* 203:2145–55

McAdam AJ, Chang TT, Lumelsky AE *et al.* (2000) Mouse inducible costimulatory molecule (ICOS) expression is enhanced by CD28 costimulation and regulates differentiation of CD4+ T cells. *J Immunol* 165:5035–40

Meyers JH, Ryu A, Monney L *et al.* (2002) Cutting edge: CD94/NKG2 is expressed on Th1 but not Th2 cells and costimulates Th1 effector functions. *J Immunol* 169:5382–6

Monney L, Sabatos CA, Gaglia JL *et al.* (2002) Th1-specific cell surface protein Tim-3 regulates macrophage activation and severity of an autoimmune disease. *Nature* 415:536–41

Nolte MA, van Olffen RW, van Gisbergen KP *et al.* (2009) Timing and tuning of CD27-CD70 interactions: the impact of signal strength in setting the balance between adaptive responses and immunopathology. *Immunol Rev* 229:216–31

Nuriya S, Enomoto S, Azuma M (2001) The role of CTLA-4 in murine contact hypersensitivity. *J Invest Dermatol* 116:764–8

Oshima H, Nakano H, Nohara C *et al.* (1998) Characterization of murine CD70 by molecular cloning and mAb. *Int Immunol* 10:517–26

Peperzak V, Xiao Y, Veraar EA *et al.* (2010) CD27 sustains survival of CTLs in virus-infected nonlymphoid tissue in mice by inducing autocrine IL-2 production. *J Clin Invest* 120:168–78

Rowley TF, Al-Shamkhani A (2004) Stimulation by soluble CD70 promotes strong primary and secondary CD8+ cytotoxic T cell responses *in vivo*. *J Immunol* 172:6039–46

Sallusto F, Lenig D, Mackay CR *et al.* (1998) Flexible programs of chemokine receptor expression on human polarized T helper 1 and 2 lymphocytes. *J Exp Med* 187:875–83

Sanchez PJ, McWilliams JA, Haluszczak C *et al.* (2007) Combined TLR/CD40 stimulation mediates potent cellular immunity by regulating dendritic cell expression of CD70 *in vivo*. *J Immunol* 178:1564–72

Soares H, Waechter H, Glaichenhaus N *et al.* (2007) A subset of dendritic cells induces CD4+ T cells to produce IFN-gamma by an IL-12-independent but CD70-dependent mechanism *in vivo*. *J Exp Med* 204:1095–106

Sumi T, Ishida W, Ojima A *et al.* (2008) CD27 and CD70 do not play a critical role in the development of experimental allergic conjunctivitis in mice. *Immunol Lett* 119:91–6

Szabo SJ, Dighe AS, Gubler U *et al.* (1997) Regulation of the interleukin (IL)-12R beta 2 subunit expression in developing T helper 1 (Th1) and Th2 cells. *J Exp Med* 185:817–24

Taraban VY, Rowley TF, Al-Shamkhani A (2004) Cutting edge: a critical role for CD70 in CD8 T cell priming by CD40-licensed APCs. *J Immunol* 173:6542–6

Tesselaar K, Xiao Y, Arens R *et al.* (2003) Expression of the murine CD27 ligand CD70 *in vitro* and *in vivo*. *J Immunol* 170:33–40

van Gisbergen KP, van Olffen RW, van Beek J *et al.* (2009) Protective CD8 T cell memory is impaired during chronic CD70-driven costimulation. *J Immunol* 182:5352–62

van Oosterwijk MF, Juwana H, Arens R *et al.* (2007) CD27-CD70 interactions sensitise naive CD4+ T cells for IL-12-induced Th1 cell development. *Int Immunol* 19:713–8

Wang B, Fujisawa H, Zhuang L *et al.* (2000) CD4+ Th1 and CD8+ type 1 cytotoxic T cells both play a crucial role in the full development of contact hypersensitivity. *J Immunol* 165:6783–90

Watanabe N, Arase H, Kurasawa K *et al.* (1997) Th1 and Th2 subsets equally undergo Fas-dependent and -independent activation-induced cell death. *Eur J Immunol* 27:1858–64

Watts TH (2005) TNF/TNFR family members in costimulation of T cell responses. *Annu Rev Immunol* 23:23–68

Wills-Karp M (1999) Immunologic basis of antigen-induced airway hyperresponsiveness. *Annu Rev Immunol* 17:255–81

Xiao Y, Peperzak V, Keller AM *et al.* (2008) CD27 instructs CD4+ T cells to provide help for the memory CD8+ T cell response after protein immunization. *J Immunol* 181:1071–82

Xu D, Chan WL, Leung BP *et al.* (1998) Selective expression and functions of interleukin 18 receptor on T helper (Th) type 1 but not Th2 cells. *J Exp Med* 188:1485–92

Research article

Severe dermatitis with loss of epidermal Langerhans cells in human and mouse zinc deficiency

Tatsuyoshi Kawamura,[1] Youichi Ogawa,[1] Yuumi Nakamura,[1] Satoshi Nakamizo,[2] Yoshihiro Ohta,[3] Hajime Nakano,[4] Kenji Kabashima,[2] Ichiro Katayama,[5] Schuichi Koizumi,[6] Tatsuhiko Kodama,[3] Atsuhito Nakao,[7] and Shinji Shimada[1]

[1]Department of Dermatology, Faculty of Medicine, University of Yamanashi, Yamanashi, Japan. [2]Department of Dermatology, Kyoto University Graduate School of Medicine, Kyoto, Japan. [3]Laboratory for Systems Biology and Medicine, Research Center for Advanced Science and Technology, University of Tokyo, Tokyo, Japan. [4]Department of Dermatology, Hirosaki University Graduate School of Medicine, Hirosaki, Japan. [5]Department of Dermatology, Osaka University School of Medicine, Osaka, Japan. [6]Department of Pharmacology and [7]Department of Immunology, Faculty of Medicine, University of Yamanashi, Yamanashi, Japan.

Zinc deficiency can be an inherited disorder, in which case it is known as acrodermatitis enteropathica (AE), or an acquired disorder caused by low dietary intake of zinc. Even though zinc deficiency diminishes cellular and humoral immunity, patients develop immunostimulating skin inflammation. Here, we have demonstrated that despite diminished allergic contact dermatitis in mice fed a zinc-deficient (ZD) diet, irritant contact dermatitis (ICD) in these mice was more severe and prolonged than that in controls. Further, histological examination of ICD lesions in ZD mice revealed subcorneal vacuolization and epidermal pallor, histological features of AE. Consistent with the fact that ATP release from chemically injured keratinocytes serves as a causative mediator of ICD, we found that the severe ICD response in ZD mice was attenuated by local injection of soluble nucleoside triphosphate diphosphohydrolase. In addition, skin tissue from ZD mice with ICD showed increased levels of ATP, as did cultured wild-type keratinocytes treated with chemical irritants and the zinc-chelating reagent TPEN. Interestingly, numbers of epidermal Langerhans cells (LCs), which play a protective role against ATP-mediated inflammatory signals, were decreased in ZD mice as well as samples from ZD patients. These findings suggest that upon exposure to irritants, aberrant ATP release from keratinocytes and impaired LC-dependent hydrolysis of nucleotides may be important in the pathogenesis of AE.

Introduction

Zinc (Zn) is a trace element essential for cell growth, development, and differentiation and is involved in maintaining the structure and function of over 300 different enzymes (1, 2). More than 2,000 transcription factors regulating gene expression require Zn for their structural integrity and binding to DNA (3). Recent studies revealed that Zn acts as an intracellular second messenger for transducing extracellular stimuli into intracellular signaling events in monocytes, DCs, and mast cells (4–7).

Zn deficiencies can be divided into 2 groups – a congenital form, called acrodermatitis enteropathica (AE; OMIM 201100), and the acquired forms (8). Recently, mutations in SLC39A4 have been identified as being responsible for congenital AE (9–11). SLC39A4 encodes ZIP4 Zn transporter, which is involved in Zn uptake via transporting Zn into the cytoplasm in intestine (9, 10). Congenital AE occurs worldwide, with an estimated incidence of 1 per 500,000 children, while it has been estimated that more than 2×10^9 people have a nutritional deficiency for Zn in developing countries (3, 8). It is even estimated that a considerable proportion of the Western population is at risk of marginal Zn deficiency (12, 13). Conditional Zn deficiencies also occur in many diseases and abnormal conditions, including malabsorption syndrome, chronic liver and renal diseases, sickle cell disease, excessive intake of alcohol, malignancies, and other chronic debilitating conditions (1, 3, 8).

The clinical manifestations of inherited and acquired Zn deficiency include growth retardation, diarrhea, alopecia, and characteristic skin lesions on acral, periorificial, and anogenital areas. Since Zn is indispensable for an adequate immunological response to all pathogens (14), the most serious complication observed in Zn deficiency is repeated infections due to impaired immune function. Indeed, several studies using animal models of Zn deficiency have confirmed that decreased levels of Zn induce thymic atrophy, lymphopenia, and compromised cell- and antibody-mediated immune responses (14, 15). Zn deficiency affects many aspects of immune function, including a shift of the Th cell response to a Th2 predominance, reduced antibody formation, reduced killing activity by NK cells and lower levels of phagocytosis and intracellular killing in granulocytes, monocytes, and macrophages (14–18). Zn also influences the production of chemokines and proinflammatory cytokines like TNF-α, IL-1β, and IL-6 (19–22).

The effects of Zn deficiency are particularly obvious in the skin and are seen as erythematous rashes, scaly plaques, and ulcers on acral and periorificial areas. Paradoxically, despite the impaired immune function in Zn deficiency, patients with hereditary and acquired AE present with immunostimulating skin inflammation, known as "acrodermatitis." It remains unclear which cellular processes induce this characteristic skin inflammation and account for the cutaneous pathological features of Zn deficiency (8). Here we investigated the mechanisms by which Zn deficiency induces dermatitis in AE using dietary Zn-deficient (ZD) mice.

Conflict of interest: The authors have declared that no conflict of interest exists.
Citation for this article: *J Clin Invest* doi:10.1172/JCI58618.